



Comprehensive taxon sampling and vetted fossils help clarify the time tree of shorebirds (Aves, Charadriiformes)

David Černý^{a,*}, Rossy Natale^b

^a Department of the Geophysical Sciences, University of Chicago, Chicago 60637, USA

^b Department of Organismal Biology & Anatomy, University of Chicago, Chicago 60637, USA



ARTICLE INFO

Keywords:

Phylogeny
Birds
Charadriiformes
Fossil calibrations
Macroevolution

ABSTRACT

Shorebirds (Charadriiformes) are a globally distributed clade of modern birds and, due to their ecological and morphological disparity, a frequent subject of comparative studies. While molecular phylogenies have been key to establishing the suprafamilial backbone of the charadriiform tree, a number of relationships at both deep and shallow taxonomic levels remain poorly resolved. The timescale of shorebird evolution also remains uncertain as a result of extensive disagreements among the published divergence dating studies, stemming largely from different choices of fossil calibrations. Here, we present the most comprehensive non-supertree phylogeny of shorebirds to date, based on a total-evidence dataset comprising 353 ingroup taxa (90% of all extant or recently extinct species), 27 loci (15 mitochondrial and 12 nuclear), and 69 morphological characters. We further clarify the timeline of charadriiform evolution by time-scaling this phylogeny using a set of 14 up-to-date and thoroughly vetted fossil calibrations. In addition, we assemble a taxonomically restricted 100-locus dataset specifically designed to resolve outstanding problems in higher-level charadriiform phylogeny. In terms of tree topology, our results are largely congruent with previous studies but indicate that some of the conflicts among earlier analyses reflect a genuine signal of pervasive gene tree discordance. Monophyly of the plovers (Charadriidae), the position of the ibisbill (*Ibidorhyncha*), and the relationships among the five subfamilies of the gulls (Laridae) could not be resolved even with greatly increased locus and taxon sampling. Moreover, several localized regions of uncertainty persist in shallower parts of the tree, including the interrelationships of the true auks (Alcinae) and anarhynchine plovers. Our node-dating and macroevolutionary rate analyses find support for a Paleocene origin of crown-group shorebirds, as well as exceptionally rapid recent radiations of Old World oystercatchers (Haematopodidae) and select genera of gulls. Our study underscores the challenges involved in estimating a comprehensively sampled and carefully calibrated time tree for a diverse avian clade, and highlights areas in need of further research.

1. Introduction

Shorebirds (Charadriiformes) are an ecologically diverse and globally distributed order of more than 380 species of neoavian birds (Boyd, 2019; Clements et al., 2020). Given the variation in habitat use, foraging mode, and behavior present in the group, the Charadriiformes have been a frequent subject of comparative research. A number of studies have investigated the origins and macroevolution of ecological, behavioral, or phenotypic traits in specific charadriiform genera or families, shedding light on questions such as the evolution of beak morphology in the Charadrii and Scolopacidae (Barbosa and Moreno, 1999), locomotor ecologies in auks and relatives (Smith and Clarke, 2012), migration

behaviors in the *Charadrius* plovers (Joseph et al., 1999), and plumage in gulls and terns (Crochet et al., 2000; Bridge et al., 2005; Dufour et al., 2020). Despite these efforts, comparative analyses of shorebird morphology, ecology, and behavior at the ordinal level have been hampered by the lack of a robust, comprehensive time-calibrated phylogeny for the clade as a whole.

A division of Charadriiformes into three suborders has become well-established since molecular data started to replace or supplement the osteological (Strauch, 1978; Björklund, 1994; Chu, 1995), syringeal (Brown and Ward, 1990), integumentary (Jehl, 1968, 1975, 2000), and behavioral (Moynihan, 1959) characters that were used (often together, e.g. Chu, 1998; Jehl, 1968) to generate the earliest hypotheses of

* Corresponding author.

E-mail address: david.cerny1@gmail.com (D. Černý).

charadriiform phylogenetic relationships. This three-suborder structure consists of the Charadrii (plovers, thick-knees, oystercatchers, avocets), Scolopaci (jacanas, sandpipers, snipes), and the Lari (gulls, auks, skuas, coursers). This basic structure was first identified by the DNA-DNA hybridization work of [Sibley and Ahlquist \(1990\)](#), which also helped resolve the position of several taxa whose charadriiform affinities had been controversial, such as the auks ([Verheyen, 1958; Gysels and Rabaey, 1964](#)) and the plains-wanderer ([Wetmore, 1960; Cracraft, 1981](#)). The inclusion of the auks within Lari suggested by [Sibley and Ahlquist \(1990\)](#) agreed with earlier hypotheses suggesting their close relationship to the gulls ([Storer, 1960; Kozlova, 1961](#)), while a sister-group relationship between the plains-wanderer and seedsnipes within Scolopaci corroborated the earlier morphological study of [Olson and Steadman \(1981\)](#). Topology-wise, [Sibley and Ahlquist \(1990\)](#) found the Scolopaci as the sister group of (Charadrii + Lari). Later studies using sequence data altered this topology by placing the Charadrii as sister to a clade formed by the Scolopaci and Lari, and by recovering the enigmatic buttonquails (Turnicidae), previously considered to be either gruiforms ([Wetmore, 1960; Cracraft, 1981; Rotthowe and Starck, 1998](#)) or a separate early-branching neoavian order ([Sibley and Ahlquist, 1990](#)), as early-diverging members of the Lari ([Paton et al., 2003; Cracraft et al., 2004; Fain and Houde, 2004, 2007; Paton and Baker, 2006; Baker et al., 2007; Hackett et al., 2008; Prum et al., 2015; Hu et al., 2017; Kuhl et al., 2020](#)).

Despite this general consensus, there remain several outstanding questions regarding higher-level charadriiform phylogenetic relationships, some of which concern the position of several monotypic families. The ibisbill (*Ibidorhyncha struthersii*) has been recovered as the sister group to the Recurvirostridae in morphological ([Chu, 1995; Livezey, 2010](#)) and supertree ([Thomas et al., 2004](#)) studies, while molecular analyses have allied it with the Haematopodidae ([Baker et al., 2007; Chen et al., 2018](#)) or a (Haematopodidae + Recurvirostridae) clade ([Burleigh et al., 2015](#)). The monotypic crab plover (*Dromas ardeola*) was not represented in the early molecular phylogenetic studies on charadriiforms ([Paton et al., 2003; Paton and Baker, 2006; Baker et al., 2007; Fain and Houde, 2007](#)), and larger phylogenomic studies that did include it failed to sample shorebirds densely enough to unambiguously resolve its position within the order ([Hackett et al., 2008; Reddy et al., 2017](#)). Recent molecular evidence indicates a sister-group relationship

of *Dromas* to the coursers and pratincoles (Glareolidae), albeit with varying degrees of support ([Pereira and Baker, 2010; Burleigh et al., 2015; De Pietri et al., 2020](#); see also the supertree of [Kimball et al. \(2019\)](#)). Finally, the monophyly of lapwings and plovers (Charadriidae) has been contested, with multiple studies finding the gray and golden plovers (genus *Pluvialis*) to be more closely related to the Haematopoidea than to the rest of the family ([Baker et al., 2007; Fain and Houde, 2007; Burleigh et al., 2015; Chen et al., 2018](#)), or to fall outside of the clade formed by the Haematopoidea and other plovers ([Ericson et al., 2003](#)). This contradicts the traditional morphological hypothesis of charadriid monophyly ([Chu, 1995; Livezey, 2010](#)) as well as the nuclear sequence analysis of [Baker et al. \(2012\)](#), who attributed the earlier molecular results to stochastic gene tree estimation error stemming primarily from the use of fast-evolving mitochondrial loci. However, phylogenies based on complete mitogenomes have since recovered *Pluvialis* within the Charadriidae ([Hu et al., 2017; Chen et al., 2018](#)), whereas the taxonomically comprehensive analysis of [Burleigh et al. \(2015\)](#), in which the position of *Pluvialis* was informed by three nuclear loci in addition to mtDNA data, again supported plover paraphyly.

The timescale of charadriiform evolution also remains uncertain due to incongruence among studies employing different types of molecular data and different interpretations of the fossil record. Notably, there is a threefold difference between the oldest (95% credible interval: 68–107 Ma; [Paton et al., 2003](#)) and the youngest (95% credible interval: 35.1–60.3 Ma; [Prum et al., 2015](#)) estimates of the age of the charadriiform crown (Fig. 1), with the two values implying drastically different scenarios for the tempo and mode of shorebird diversification. Early molecular dating studies based on mitochondrial DNA or small samples of nuclear loci placed the origin of crown shorebirds deep in the Late Cretaceous ([Paton et al., 2002; Paton et al., 2003; Pereira and Baker, 2006](#)), and in some cases suggested that many of their interfamilial divergences predated the Cretaceous–Paleogene (K–Pg) boundary ([Baker et al., 2007; Brown et al., 2007; Brown et al., 2008; Pereira and Baker, 2008](#)). These divergence time estimates are incompatible with the lack of any Cretaceous fossils that could be reliably attributed not only to charadriiforms ([Smith, 2015](#)), but even to neoavians in general ([Field et al., 2020](#)), and with phylogenomic evidence for an explosive origin of neoavian orders that largely ([Ericson et al., 2006; Jarvis et al., 2014; Kimball et al., 2019; Kuhl et al., 2020](#)) or perhaps entirely ([Claramunt](#)

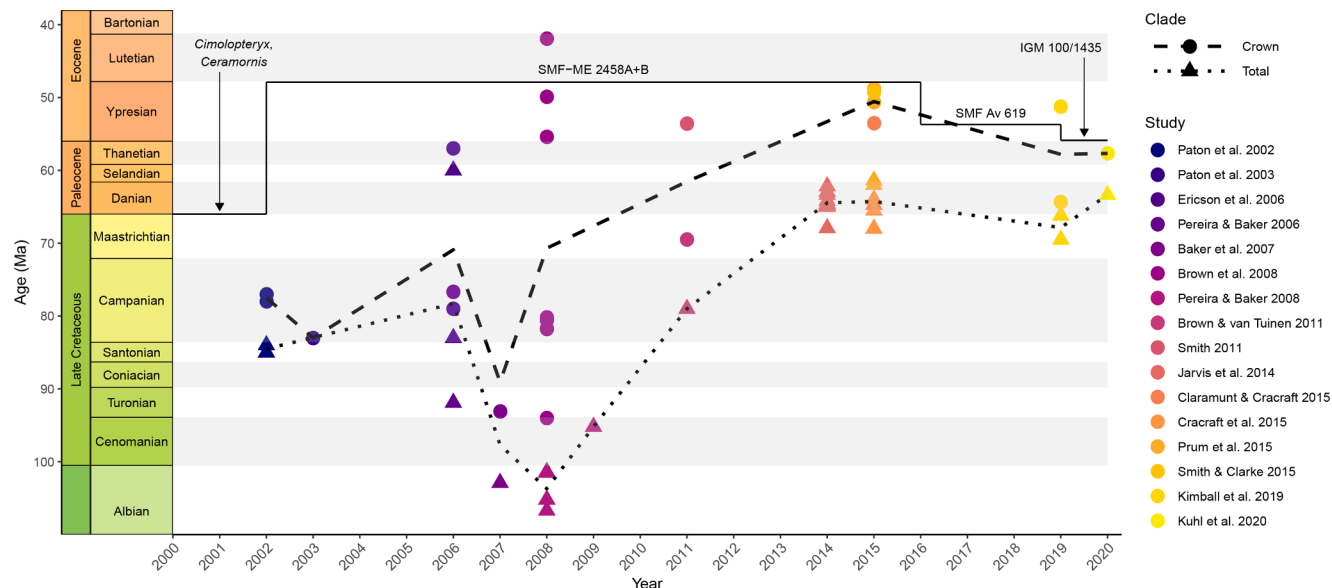


Fig. 1. Previous age estimates for the Charadriiformes, plotted against the publication year and the oldest crown-charadriiform fossil known at the time (solid line). Mean estimates across different studies are shown separately for the total group (dotted line) and crown group (dashed line). After a long period during which the molecular divergence times drastically predated the known fossil record, the converse problem has started to occur with the advent of phylogenomic studies in the mid-2010s. See References for the full citations of the studies shown.

and Cracraft, 2015; Cracraft et al., 2015; Prum et al., 2015) postdated the K-Pg boundary, reflecting a rapid radiation into the ecological niches emptied by the Cretaceous–Paleogene mass extinction (Ksepka and Phillips, 2015; Suh, 2016; Berv and Field, 2017).

In part, the implausibly old divergence times inferred by early analyses can be attributed to the reliance on mitochondrial data (Brown and van Tuinen, 2011), which frequently overestimate node ages as a result of substitution saturation and small effective population sizes (Zheng et al., 2011; Smith and Klicka, 2013). However, inadequate calibration choices also play a role (Mayr, 2011; Smith, 2015). A number of early studies relied primarily on external calibrations phylogenetically distant from the clade of interest (Paton et al., 2002; Pereira and Baker, 2006), or re-used previous and excessively old divergence time estimates as secondary calibrations (Paton et al., 2003). The choice of calibration points within the Charadriiformes has been equally problematic, as the relevant taxa were drawn from obsolete fossil compilations without considering more recent re-assessments. Thus, Baker et al. (2007) calibrated the split between charadriiforms and their sister group with the ~66 Ma old taxa *Ceramornis* and *Cimoloptyyx*, which were regarded as charadriiforms by Brodkorb (1967) but subsequently re-evaluated as crown birds (Neornithes) of uncertain affinities by Hope (2002). Moreover, both fossils may be either latest Cretaceous or early Paleocene in age (Mayr, 2009), making them poorly constrained both phylogenetically and stratigraphically. Similar problems extended to nearly all calibrations used by Baker et al. (2007) and Pereira and Baker (2008) (see Mayr, 2011; Smith, 2011 for detailed criticisms), rendering the resulting divergence time estimates untrustworthy.

More recent node-dating analyses have generally inferred much younger divergence times for the Charadriiformes (Fig. 1), estimating their origin to be younger than the K-Pg boundary (Jarvis et al., 2014; Kuhl et al., 2020) and often as young as Eocene in age (Claramunt and Cracraft, 2015; Prum et al., 2015; Kimball et al., 2019). While this shift

to younger dates may have been aided by the transition to more slowly evolving and less saturated nuclear loci, as well as by the smaller branch length estimation error resulting from the use of larger quantities of sequence data (Yang and Rannala, 2005), the fact that a similar estimate was obtained by a study using a short mtDNA-dominated alignment along with carefully vetted calibrations (Smith and Clarke, 2015) points to calibration choice as the decisive factor. Indeed, a number of recent phylogenomic studies have cited and followed the “best practices” outlined by Parham et al. (2011), according to which calibrations should be assigned to nodes based on a list of apomorphies or the results of phylogenetic analysis, and explicit reasoning should be provided for the conversion of the available stratigraphic information into numeric ages. However, an overly conservative interpretation of these guidelines may have caused recent studies to over-correct and disregard pertinent fossil evidence, possibly resulting in the underestimation of divergence times (Fig. 1). In the worst case, this bias may even give rise to “zombie lineages” (*sensu* Springer et al., 2017) whose estimated divergence time postdates their first appearance in the fossil record. For example, Jarvis et al. (2014) used the ~32 Ma old *Boutersemia* to calibrate the divergence of the Charadriiformes from their sister group, despite the fact that an almost 50% older fossil had already been described by Mayr (2000) and assigned to the Charadriiformes based on apomorphies determined by outgroup comparison. Other fossils older than 32 Ma had been recovered as crown-group charadriiforms in a formal phylogenetic analysis by Smith (2011), demonstrating that even this more stringent criterion did not justify basing the calibration on *Boutersemia*.

Near-complete species-level phylogenies are increasingly available for many avian clades (e.g. Garcia-R et al., 2014; Marki et al., 2017; Olsson and Alström, 2020), providing a robust basis for inferences ranging from diversification rate estimation to historical biogeography. In shorebirds, however, such phylogenies (summarized in Fig. 2) remain subject to methodological shortcomings and limited data availability.

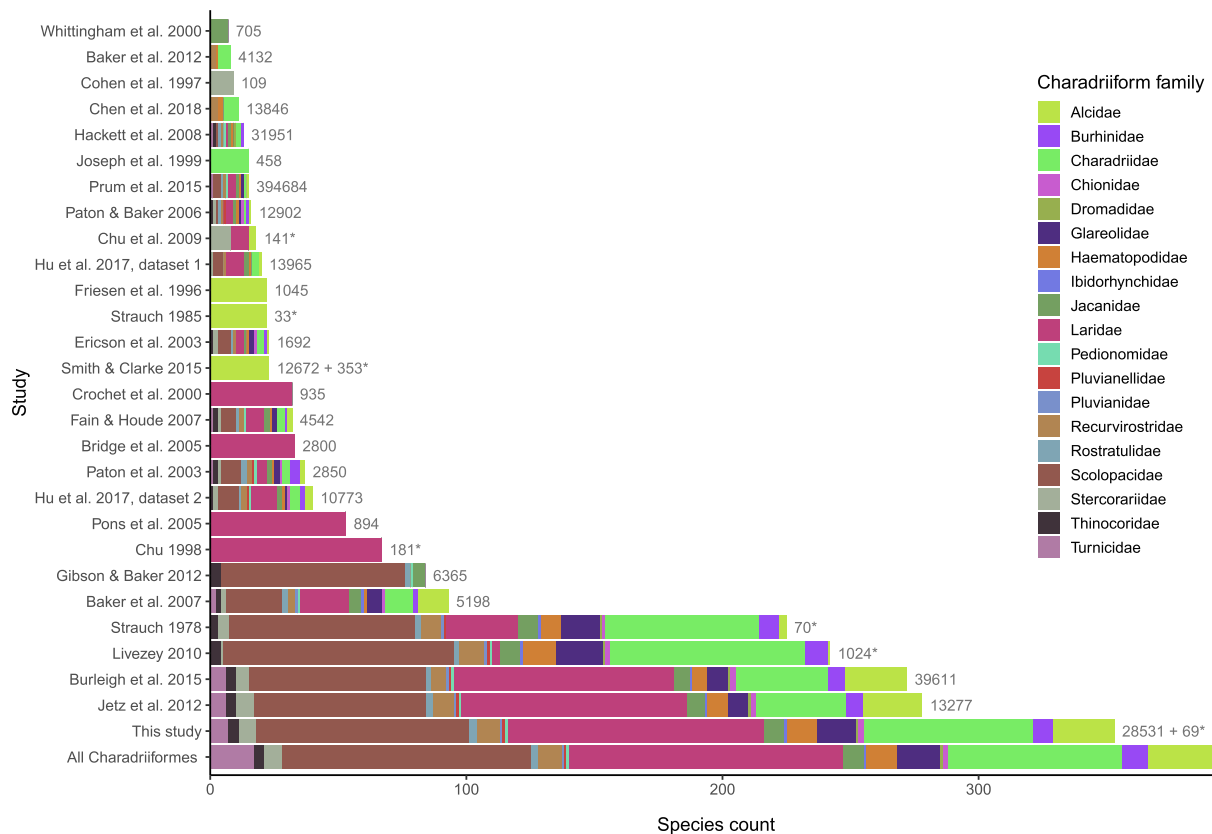


Fig. 2. Taxonomic coverage of previous phylogenetic analyses of the Charadriiformes. Outgroups were not included in counts of family-level coverage. Bars are labeled with the number of characters used; asterisks denote morphological characters. See References for the full citations of the studies shown.

With 227 species, the charadriiform matrix of Strauch (1978) still represents one of the largest morphological phylogenetic datasets ever constructed in terms of the number of taxa, but this early achievement has not been followed by subsequent morphological and molecular studies, whose taxon sampling has mostly remained either broad but sparse (Baker et al., 2007; Mayr, 2011) or dense but narrow (Cohen et al., 1997; Whittingham et al., 2000; Pons et al., 2005; Chu et al., 2009; Smith and Clarke, 2015). As a result, attempts to construct a comprehensive shorebird phylogeny have so far relied on supertree techniques. The supertree of Thomas et al. (2004) succeeded at including all 350 then-recognized non-turricid species, but aside from problems inherent to the method used (Gatesy and Springer, 2004; Bininda-Emonds, 2014), it also suffered from poor resolution and the reliance on obsolete source trees incompatible with the emerging consensus about shorebird phylogeny. Using a more advanced “backbone-and-patch” approach, Jetz et al. (2012) first inferred separate time trees for Charadrii, Scolopaci, Turnicidae, and Larida from sequence data, and attached them to a phylogenomic backbone to produce a set of phylogenies comprising a total of 278 charadriiform species. These were then expanded to all 369 then-recognized species by using taxonomy to constrain the placement of those taxa for which no molecular data were available, and stochastically resolving the resulting polytomies. While accommodating uncertainty better than the approach of Thomas et al. (2004), this workflow, too, suffers from important drawbacks. The information about topology and divergence times present in the sequence data is not allowed to inform the backbone, and the placement of many taxa (> 25% of the extant charadriiform diversity) is not based on actual data and may reproduce the errors of previous taxonomies. Moreover, the use of birth-death polypomy resolvers may lead to unreliable downstream inferences (Rabosky, 2015; Weedop et al., 2019). The more recent phylogeny of Burleigh et al. (2015), based on a single molecular supermatrix, avoided these problems at the cost of reduced taxon sampling (272 charadriiform species; Fig. 2).

Here, we assemble the most comprehensive molecular dataset for the Charadriiformes to date, and combine it with a pre-existing morphological character matrix to estimate the phylogenetic interrelationships of 353 species of shorebirds (~90% of the known extant or recently extinct species). This taxon sample exceeds that of any previous study not based on data-free polypomy resolvers (Fig. 2), making it possible to address outstanding areas of uncertainty due to insufficient sampling. Furthermore, we combine the resulting comprehensive total-evidence phylogeny with an up-to-date, extensively vetted set of 14 fossil calibrations to resolve the controversial timescale of shorebird evolution, shedding light on the tempo and mode of charadriiform diversification.

2. Materials and methods

2.1. Data assembly and alignment

We obtained published sequences from GenBank (Benson et al., 2017) and BOLD (Ratnasingham and Hebert, 2007) using Geneious (Kearse et al., 2012) or manual queries. We further included several unpublished sequences from Dos Remedios et al. (2015) that were too short to be deposited in GenBank, an as-yet undeposited CytB sequence of the Madagascan jacana (*Actophilornis albinucha*; D'Urban Jackson et al., 2019), and a recently published but undeposited COI sequence of Saunders's tern (*Sternula saundersi*; Almalki et al., 2021). Additional sequences for the nuclear loci were obtained from the whole-genome scaffolds generated by the B10K project (Feng et al., 2020) and other ongoing sequencing efforts by BLASTing existing samples against the NCBI wgs database using BLASTn 2.12.0+. To ensure all available sequences were obtained, taxonomic coverage was further checked against previous molecular phylogenies attempting to comprehensively sample charadriiforms and their individual subclades (Bridge et al., 2005; Gibson and Baker, 2012; Burleigh et al., 2015; Dos Remedios et al., 2015). Several sequences were excluded *a priori* based on

previously reported problems (Sangster and Luksenburg, 2021; Päckert, 2022; Laurent Raty pers. comm.) including misidentification, chimeric assembly, or sequencing errors (Appendix A, Table A.2). Whenever multiple conspecific accessions were available, the longest sequence was used unless otherwise problematic.

Our taxonomy followed the Taxonomy in Flux (TiF) checklist (Boyd, 2019) (v3.05 from August 2019), with the following exceptions: the Magellanic snipe *Gallinago magellanica* was split from the South American snipe *Gallinago paraguaiae* following Miller et al. (2020), the Eastern Eurasian oystercatcher *Haematopus osculans* was split from the Western Eurasian oystercatcher *Haematopus ostralegus* following Senfeld et al. (2020), the short-billed gull *Larus brachyrhynchus* was split from the common gull *Larus canus* following the American Ornithological Society (Chesser et al., 2021), the white-faced plover *Ochthodromus dealbatus* was split from the Kentish plover *Ochthodromus alexandrinus* following Sadanandan et al. (2019) and Wang et al. (2019b), and the West African crested tern *Thalasseus albидorsalis* was split from the royal tern *Thalasseus maximus* following the American Ornithological Society (Chesser et al., 2020). In contrast, following Senfeld et al. (2020), we did not consider *Haematopus meadowaldoi* to represent a species distinct from *Haematopus ostralegus* (though see Collar et al., 2021), and we treated *Prosobonia ellisi* as a junior synonym of *Prosobonia leucoptera* following Jansen et al. (2021). Finally, we preferred the spelling *Vanellus malabaricus* for the scientific name of the yellow-wattled lapwing following Dickinson and Remsen (2013). In total, we recognized 391 extant or recently extinct species. The reconciliation of the NCBI taxonomy with the TiF checklist was performed manually.

To date, phylogenomic analyses have not conclusively identified the sister group of shorebirds (Hackett et al., 2008; Kimball et al., 2013; McCormack et al., 2013; Yuri et al., 2013; Jarvis et al., 2014; Burleigh et al., 2015; Prum et al., 2015; Reddy et al., 2017; Kuhl et al., 2020). The Charadriiformes represent one of the six (Houde et al., 2019) to nine (Suh, 2016) major neoavian lineages whose interrelationships remain unresolved even with genome-scale data (Bravo et al., 2021), and which may constitute a hard polypomy (Suh et al., 2015; Suh, 2016). Here, we chose a gruiform species as the outgroup, as the Gruiformes were found to be the sister group of shorebirds in two recent genome-scale analyses (Jarvis et al., 2014; Kuhl et al., 2020). This hypothesis is also supported by phylogenetic analyses of phenotypic data from extant taxa (McKittrick, 1991; Livezey and Zusi, 2007) and a high degree of morphological similarity between the early members of both clades (Musser and Clarke, 2020). To maximize data coverage for this outgroup, we specifically selected the gray-crowned crane (*Balearica regulorum*), a taxon for which both the complete nuclear genome (Zhang et al., 2014) and the complete mitochondrial genome (Krajewski et al., 2010) are available.

In assembling our dataset, we prioritized the number of available sequences, and accordingly required more than 15 species to be sampled for each gene (not counting the BLAST hits) to exclude low-coverage loci. The final sample included 2 mitochondrial ribosomal genes, 13 mitochondrial protein-coding genes, and 11 nuclear protein-coding genes represented by intronic and/or exonic sequences (Table 1). We aligned the sequences using MUSCLE (Edgar, 2004) as implemented in Geneious (Kearse et al., 2012), and further refined them using the standalone version of the program if necessary. Reading frames in exonic sequences were identified using amino acid translation and were employed to check for poorly aligned sequences.

In addition to molecular data, we also employed the morphological matrix of Strauch (1978), which we modified following the recommendations of Chu (1995). Due to taxonomic changes that have taken place since the publication of the original matrix, there were several instances in which a single operational taxonomic unit (OTU) corresponded to multiple currently recognized species (e.g., *Thalasseus sandvicensis* → *Thalasseus sandvicensis* + *Thalasseus acuflavidus*), or in which multiple OTUs corresponded to a single valid species (e.g., *Haematopus palliatus* + “*Haematopus frazari*” → *Haematopus palliatus*). To avoid the accidental creation of chimeras combining morphological data

Table 1

Information for the 27 markers used to construct the concatenated alignment. The table includes alignment length, number of sequences available (based on the TiF taxonomy and after the exclusion of conspecifics), and average pairwise identity.

Code	Gene	Aligned length (bp)	Species sampled	Avg. pairwise identity (%)
<i>Mitochondrial</i>				
12S	12S ribosomal RNA	1081	222	85.1
16S	16S ribosomal RNA	1781	133	84.7
ATP6	ATP synthase membrane subunit 6	674	125	83.2
ATP8	ATP synthase membrane subunit 8	174	122	79.9
COI	Cytochrome c oxidase subunit I	1554	312	86.0
COII	Cytochrome c oxidase subunit II	684	94	85.8
COIII	Cytochrome c oxidase subunit III	787	97	87.1
CytB	Cytochrome b	1148	277	83.6
ND1	NADH dehydrogenase subunit 1	982	105	82.9
ND2	NADH dehydrogenase subunit 2	1049	232	81.7
ND3	NADH dehydrogenase subunit 3	353	123	84.0
ND4	NADH dehydrogenase subunit 4	1374	91	83.2
ND4L	NADH dehydrogenase subunit 4L	297	89	84.4
ND5	NADH dehydrogenase subunit 5	1825	117	83.4
ND6	NADH dehydrogenase subunit 6	525	95	82.8
<i>Nuclear</i>				
ADH	Alcohol dehydrogenase 1, exons 5–6	916	87	89.4
ALDOB	Fructose-bisphosphate aldolase B, exons 3–8	2287	57	85.7
BDNF	Brain-derived neurotrophic factor	688	48	97.9
CMOS	Oocyte maturation factor Mos	999	60	93.5
FGB	Fibrinogen beta-chain, introns 6–7	2009	106	84.1
GAPDH3–5	Glyceraldehyde-3-phosphate dehydrogenase, introns 3–5	817	55	83.2
GAPDH11	Glyceraldehyde-3-phosphate dehydrogenase, intron 11	526	88	84.4
MB2	Myoglobin, intron 2	814	91	91.9
MUSK	Muscle skeletal receptor tyrosine kinase, intron 4	687	48	89.0
NTF3	Neurotrophin-3	728	54	97.0
ODC	Ornithine decarboxylase, introns 6–7	768	62	87.3
RAG1	Recombination activating gene 1	3004	196	93.5

from one species with molecular data from another species, we excluded the former OTUs from the matrix. The latter OTUs were merged and any differences between the original codings were re-scored as polymorphisms. After these modifications, the matrix comprised a total of 69 characters scored for 218 taxa (original matrix: 70 characters, 227 taxa), including 60 parsimony-informative characters and 9 autapomorphies. Unlike the molecular alignment, the morphological matrix did not include an outgroup nor any representatives of the buttonquails (Turnicidae).

2.2. Gene tree analyses

We subjected the 27 individual locus alignments to multiple iterations of tree searches to identify mislabeled or chimerical sequences. Preliminary maximum-likelihood (ML) gene trees were inferred using RAxML-NG (Kozlov et al., 2019) under the general time-reversible model with discrete gamma-distributed among-site rate variation (GTR+Γ), no partitioning, and 100 tree searches based on 50 random and 50 parsimony-based starting trees. The resulting trees were inspected following the criteria broadly based on those of Sangster and Luksenburg (2021). We checked for unusually long branches, suspicious placement (e.g., a species of one genus deeply nested within another genus), and conflicts between phylogenetic positions inferred from different mitochondrial loci. Individual sequences that violated the monophyly of traditional families were usually regarded as misplaced. However, several closely related families failed to exhibit reciprocal monophyly in multiple gene trees (Laridae and Alcidae with respect to each other and Stercorariidae; Charadriidae with respect to Haemato-podidae, Recurvirostridae, and Ibidorhynchidae), and their early-diverging representatives (e.g., *Rynchops*, *Fraterculinae*) were often separated from the remaining members of the same family by non-members. Such sequences were not excluded unless they exhibited other problems. In addition, we further monitored for gene tree misrooting, which has been shown to negatively impact phylogenomic studies (Simmons et al., 2022), following the unanimous consensus among molecular analyses that the correct root lies between a monophyletic Charadrii and all other shorebirds (Ericson et al., 2003; Baker et al., 2007; Fain and Houde, 2007; Hackett et al., 2008; Prum et al., 2015; Kuhl et al., 2020). Rooting errors were often successfully addressed by the removal of the outgroup, whose relatively short branch in the nuclear gene trees frequently caused the root to fall inside the ingroup (cf. Simmons et al., 2022), particularly within Charadrii.

The misplacement and misrooting criteria for sequence exclusion were not applied to very short loci that did not contain enough information to resolve even well-established clades, such as ATP8 with just 174 base pairs (Table 1; Appendix A, Figure A.8). For data-poor loci, the removal of problematic sequences occasionally resulted in cascading changes to the topology of the tree. In such cases, multiple tree searches were conducted to find the optimum combination of excluded taxa that maximized the number of recovered “benchmark clades” (Agnarsson and May-Collado, 2008) whose monophyly was robustly established by prior studies (Cracraft, 2013). Several instances of sequences that were misplaced or subtended by unusually long branches proved to be due to alignment errors; these were corrected by algorithmic refinement (using MUSCLE) or manual editing in AliView (Larsson, 2014), and by verifying that the RAxML-NG tree estimates exhibited higher likelihoods when inferred from the edited as opposed to original alignments. The refined and/or pruned alignments were then used for the final iteration of gene tree inference, conducted under the same settings as in the first iteration. In addition, bootstrap analysis with 1000 pseudoreplicates was performed on the final alignment of each nuclear gene.

We used DiscoVista (Sayyari et al., 2018) to assess gene tree discordance by calculating and visualizing the proportion of loci that supported the interfamilial relationships present in the concatenation-based trees. To accentuate those gene tree conflicts that might be due to genuinely different evolutionary histories of the loci analyzed, as opposed to mere stochastic or systematic error, the mitogenome was treated as a single unit for the purposes of DiscoVista analyses, since it constitutes a single nonrecombinant “superlocus” due to linkage (Reyes et al., 2004; Brown and van Tuinen, 2011; Doyle, 2022). In contrast, we opted to treat GAPDH3–5 and GAPDH11 as independent loci, since they are separated by over 1300 bp in the killdeer (*Charadrius vociferus*) genome, and recombination rates within the nuclear genome are known to be high enough for a single gene to potentially comprise multiple coalescent genes (c-genes) with independent histories (Springer and Gatesy, 2018; Doyle, 2022).

To obtain a single gene tree representative of the entire mitogenome, we used Phyluce (Faircloth, 2015) to concatenate the pruned and refined alignments for all 15 mitochondrial loci. We used the PartitionFinder algorithm (Lanfear et al., 2016) as implemented in IQ-TREE v2.1.2 (Minh et al., 2020) under the `-m TESTMERGEONLY` flag to find the best partitioning scheme by greedily merging an initial scheme partitioned by locus and by codon position for the protein-coding genes (41 partitions), evaluating the Bayesian Information Criterion (BIC) for each candidate set of partitions and substitution models. We retained the resulting best-fit scheme of 16 partitions for the subsequent maximum-likelihood analysis conducted using RAxML-NG, but modified the best-fit models to use ML rather than empirical estimates of equilibrium base frequencies, and to account for cases when the best-fit model included both the proportion of invariant sites (+I) and the Γ rate heterogeneity model (+G). Since these two parameters are not identifiable (Yang, 2014), we only employed the more flexible Γ distribution of site rates in conjunction with the preferred substitution model. Except for partitioning, the RAxML-NG settings for the main tree search and bootstrapping followed those applied to other gene tree analyses.

2.3. Concatenated analyses

We used Phyluce (Faircloth, 2015) to concatenate the pruned and refined alignments of all 27 loci, and calculated partial decisiveness (Sanderson et al., 2010) for the resulting supermatrix using the Python package SUMAC (Freyman, 2015). We again used IQ-TREE 2 to identify the best partitioning scheme, and to select the best-fitting substitution and rate heterogeneity models for the final partitions. A greedy search was initialized with a set of 135 preliminary partitions (2 for the ribosomal RNA genes, 39 for the three codon positions of the 13 mitochondrial protein-coding loci, 78 for the three codon positions of 26 nuclear exons, and 16 for nuclear introns), which were iteratively merged into 23 partitions comprising the final best scheme. As before, we passed this scheme and the selected models to RAxML-NG for a maximum-likelihood tree search, with the same settings and model modifications as in the gene tree analyses. Thorough bootstrap analysis with 1000 pseudoreplicates was performed to assess node support.

Resampling-based support measures such as nonparametric bootstrap have recently been criticized for their tendency to yield high values even in the presence of substantial intra-dataset conflict (Salichos and Rokas, 2013; Suh, 2016). To take this criticism into account, we further estimated internode certainty (IC; Salichos and Rokas, 2013; Salichos et al., 2014; Kobert et al., 2016) for our ML tree. IC is an entropy-based measure of incongruence that is calculated for a reference tree based on a collection of (partial) alternative trees. It ranges from 1 (in the absence of conflict) through 0 (if the bipartition in the reference tree is present in the same percentage of trees as the most prevalent conflicting bipartition) to negative values (if there are more frequent alternatives to the bipartition present in the reference tree; Kobert et al., 2016). Since IC is only robust as a measure of support when the collection of alternative trees is sufficiently large (Salichos et al., 2014), we chose to use the bootstrap set for this purpose, and scored the ML tree accordingly using RAxML v8.2.12 (Stamatakis, 2014) with the `-f i -t` flags.

In addition to the ML analysis, we also performed Bayesian phylogenetic inference using ExaBayes v1.5.1 (Aberer et al., 2014) via the CIPRES portal (Miller et al., 2010). We used the best partitioning scheme described above, except that individual partitions were assigned separate GTR+ Γ models rather than the optimum models selected by IQ-TREE, which were not available in ExaBayes. We linked branch lengths across partitions while placing flat Dirichlet priors on the exchangeability and state frequency vectors, a $U(0, 200)$ prior on the shape parameter of the Γ distribution, and an $Exp(10)$ prior on branch lengths (all defaults). A total of 4 independent runs were executed, each consisting of one cold and three incrementally heated Metropolis-coupled chains of 5 million generations. Topological convergence was assessed by verifying that the average standard deviation of split

frequencies (ASDSF) did not exceed 5%. In addition, following a visual inspection of trends in parameter values in Tracer v1.7 (Rambaut et al., 2018), we set burnin to 20%, combined the post-burnin portions of each run, and verified that the resulting effective sample sizes (ESS) exceeded 200 for all scalar parameters. Finally, we used the ‘consense’ utility to generate the extended majority-rule (MRE) consensus tree as a summary of the combined posterior sample.

To determine which regions of the ML and Bayesian trees may have been affected by alignment incompleteness, we used the protocol introduced by McCraney et al. (2020) to calculate per-branch locus coverage, i.e., the number of genes informative (but not necessarily supportive) with respect to a given branch. We first pruned both trees down to the species sampled for each of the 27 loci, and used ASTRAL-III v5.7.3 (Mirarab et al., 2014; Zhang et al., 2018) with the `-q` and `-t 2` flags to score and annotate the original RAxML-NG and ExaBayes trees based on the resulting set of subsampled trees. Since the pruned trees only differed from the reference trees in taxon coverage rather topology, the effective number of loci computed by ASTRAL (defined as the number of gene trees that contain one of the three possible quartets around the branch of interest; Sayyari et al., 2018) amounted to per-branch locus coverage.

2.4. Combined analyses

We employed two different methods to expand our taxon sample with species represented only by morphological data. First, we combined the concatenated alignment with the morphological character matrix of Strauch (1978), modified as described above. The resulting total-evidence supermatrix consisted of 29 partitions: 23 for the nucleotide data, delimited according to the best scheme described above; and 6 for the morphological characters, which were grouped into partitions according to the number of states (Appendix A, Table A.1). This supermatrix was then analyzed using RAxML-NG, using the previously selected models for the nucleotide partitions and appropriate M_k models (with k ranging from 2 to 8) for the morphological partitions. A Γ distribution discretized into 4 categories was used to account for among-site rate variation within all partitions except those comprising 5-state, 6-state, and 8-state morphological characters, for which the number of rate categories would have exceeded the number of characters. Since the matrix of Strauch (1978) only contained variable characters, an ascertainment bias correction (Lewis, 2001) was applied to all morphological models. We conducted 100 tree searches (with 50 random and 50 parsimony starting trees) and a bootstrap analysis with 1000 pseudoreplicates. In these total-evidence (TE) analyses, the morphological characters helped determine the overall topology of the tree by informing the relationships among taxa represented by both morphological and molecular data.

Second, we performed alternative analyses using the evolutionary placement algorithm (EPA; Berger and Stamatakis, 2010; Berger et al., 2011), in which the ML estimate from the concatenated analysis served as a fixed molecular scaffold, and the contribution of the morphological characters was limited to attaching to this scaffold the 19 species from Strauch, 1978’s (Strauch, 1978) matrix that lacked sequence data. To achieve this, we first pruned the 335-tip concatenated ML tree down to the 199 tips that were represented by both molecular and morphological data, and then used RAxML (`-f u`) to compute weights for the 69 characters based on their fit to this subsampled reference phylogeny, expressed in terms of per-site log likelihood scores (Berger et al., 2011). Since the weights were equal for all characters, we ran an unweighted EPA analysis using the `-f v` RAxML flag on the complete 335-tip scaffold. Next, we passed the resulting `.jplace` files to GAPPA (Czech et al., 2020) and ran it both with and without the `-fully-resolve` flag, which allows the edges of the scaffold tree to be split by the insertion edges according to the proximal length of the placements. If this option is not selected, all the insertions grafted onto the same edge of the scaffold tree are collected at the end of a single base edge,

potentially allowing for multifurcations. However, our analyses never placed more than two insertions onto the same scaffold edge, and thus yielded fully resolved (strictly bifurcating) trees under both settings. For clarity, we therefore refer to the resulting topologies as “split scaffold edges” and “group together” evolutionary placement trees (SSE-EPA and GT-EPA), respectively. We used a suite of likelihood tests implemented in IQ-TREE 2, including the Shimodaira-Hasegawa (SH; Shimodaira and Hasegawa, 1999) and approximately unbiased (AU; Shimodaira, 2002) tests, to compare the fit of the TE, SSE-EPA, and GT-EPA trees to the combined dataset.

2.5. Testing the positions of *Ibidorhyncha* and *Pluvialis*

We assembled an additional dataset to help resolve two of the most uncertain higher-level relationships among shorebirds: those of the ibisbill (*Ibidorhyncha struthersii*) and the four species of gray and golden plovers (genus *Pluvialis*). We subsampled the phylogenomic dataset of Prum et al. (2015) down to 100 loci and restricted its taxonomic coverage to the 16 sampled species of charadriiforms as well as a single gruiform outgroup (*Balearica regulorum*). We then expanded each of the resulting alignments with the two target taxa as well as additional species of plovers (Charadriidae) and stilts (Recurvirostridae) to increase taxon sampling in the focal region of the tree. Specifically, we BLASTed Prum et al., 2015's (Prum et al., 2015) sequences of the American oystercatcher (*Haematopus palliatus*) against the NCBI whole-genome shotgun database to obtain orthologous sequences from the killdeer (*Charadrius vociferus*; Zhang et al., 2014), white-headed stilt (*Himantopus leucocephalus*; Galla et al., 2019), ibisbill (Feng et al., 2020), Kentish plover (*Ochthodoromus alexandrinus*; Wang et al., 2019a), and unpublished, recently deposited sequences of the European golden-plover (*Pluvialis apricaria*; JAGGDV010000002–010000025 and JAGGDW010000013–010000778). These new samples were manually aligned against the original sequences using AliView, resulting in a set of expanded alignments with a mean length of 1550 bp (range: 616–2066 bp) that formed the input for two subsequent sets of analyses.

First, we obtained ML gene tree estimates for the 100 loci using RAxML-NG (under settings identical to those used in previous analyses), and conducted additional bootstrap analyses with the number of pseudoreplicates determined by the automRE bootstrapping criterion based on topological convergence (Pattengale et al., 2010). We then used the resulting gene trees as the input for ASTRAL-III, a summary species-tree method known to be statistically consistent under the multispecies coalescent (Zhang et al., 2018). Given a profile of unrooted and possibly only partially resolved gene trees, ASTRAL-III performs a limited tree search restricted to combinations of bipartitions observed in the source trees to find the species tree sharing the largest number of induced quartets with the profile. Assuming error-free gene trees, the method can correctly infer the species tree even in the presence of heavy incomplete lineage sorting (ILS) that renders concatenation-based approaches positively misleading (Mirarab et al., 2014; Mirarab et al., 2016). To minimize gene tree error, we used a custom R script (R Core Team, 2019) to collapse all branches with bootstrap support of <10%, following previous simulations that showed this cut-off to outperform both unfiltered analyses and more aggressive filtering (Zhang et al., 2018). Bootstrap pseudoreplicates were used to expand the search space but did not affect quartet scores, which were calculated from the ML estimates alone. We used the $-t 2$ flag to annotate the species tree with internal branch lengths in coalescent units (inversely proportional to the amount of gene tree discordance if the latter were due entirely to ILS) and local posterior probabilities (localPP; Sayyari and Mirarab, 2016). The localPP metric is a conservative measure of support that assumes error-free gene trees and perfect accuracy of the four subtrees surrounding the focal branch. Its value depends on the frequency with which the branch appears in the input gene trees, as well as the total number of gene trees evaluated (Sayyari and Mirarab, 2016). In addition, we used the $-t 10$ flag to test whether the null hypothesis of a

polytomy (zero-length internal branch) could be rejected for any given quartet (Sayyari and Mirarab, 2018).

Second, we used Phyluce to concatenate all 100 single-locus alignments into a supermatrix of 155,040 sites (total proportion of gaps and missing data = 1.72%), which we subjected to a partitioning analysis using IQ-TREE 2. The initial scheme consisted of 100 partitions (one for each locus), and was reduced by a greedy search to a final set of 15 partitions. After modifying the best-fit models to employ ML base frequency estimates and remove the proportion of invariant sites, we performed a partitioned ML analysis of the concatenated alignment using RAxML-NG (50 random + 50 parsimony starting trees; thorough bootstrap with 1000 pseudoreplicates).

2.6. Fossil calibrations

We assembled a total of 14 calibrations (Table 2): five from a recently published, expert-vetted compendium (Smith, 2015), two that were utilized in a previous divergence time analysis (De Pietri et al., 2020), and seven that were used here for the first time. Seven out of the 14 calibrations were described in or after 2010; four were described in or after 2015. All calibrations were thoroughly vetted to ensure compliance with the criteria of Parham et al. (2011). The seven calibrations taken from earlier studies were revised following recent geochronological and phylogenetic studies; in all cases, this resulted in changes to their numeric ages, and in three cases, the reassignment of a calibration to a different node (see Appendix A for details). We paid particular attention to the choice of the root calibration, since multiple fossils have been put forward as the earliest known record of shorebirds (Mayr, 2000; Mayr, 2016; Smith, 2015; Hood et al., 2019). In particular, recent phylogenetic analyses suggested a crown-charadriiform affinity for at least three fossils dating to the earliest Eocene (Musser and Clarke, 2020; Heingård et al., 2021). However, the trees in question either exhibited a lack of resolution within Charadriiformes or contradicted well-established molecular results, rendering the placement of the fossils within the crown inconclusive.

To assess the confidence in the phylogenetic position of the early Eocene fossils, we re-analyzed the morphological character matrix of Heingård et al. (2021) under three sets of “soft” topological constraints which fixed the relationships among most of the extant taxa but allowed

Table 2

Fossil calibrations used for divergence time estimation. Specimen numbers are given for remains belonging to extant species and fossils not assigned to a named species. t_L = minimum, t_U = maximum. Detailed justification and additional references for the choice of calibrations and their numeric ages are provided in Appendix A.

#	Fossil	Node calibrated	t_L (Ma)	t_U (Ma)
1	CASG 71892 (<i>Uria lomvia</i>)	<i>Uria lomvia</i> + <i>U. aalge</i>	2.58	23.57
2	<i>Alca stewarti</i>	<i>Alca</i> + <i>Pinguinus</i>	6.91	33.68
3	<i>Miocepphus bohaskai</i>	Crown-group Alcidae	18.1	57.54
4	LACM 18275	Crown-group Fraterculinae	9.3	44.80
5	USNM 192994, USNM 215783 (<i>Fratercula</i> aff. <i>arctica</i>)	<i>Fratercula arctica</i> + <i>F. corniculata</i>	3.92	22.55
6	GCVP 5690	Crown-group Alcoidea	34.44	69.88
7	<i>Mirolia</i> spp.	<i>Calidris</i> + <i>Arenaria</i>	12.6	37.80
8	<i>Gallinago azovica</i>	<i>Gallinago</i> + <i>Coenocorypha</i>	6.1	28.37
9	<i>Elorius</i> spp., <i>Parvelorius</i> spp.	Crown-group Scolopacidae	20.0	48.31
10	<i>Nupharanassa tolutaria</i>	Crown-group Jacanoidea	30.5	59.08
11	<i>Oligonomus milleri</i>	Crown-group Thinocoroidea	24.47	48.95
12	NMB S.G.20252	Crown-group Haematoopoidea	20.0	68.43
13	<i>Chionoides australiensis</i>	Crown-group Chionida	24.76	68.83
14	IGM 100/1435	Crown-group Charadriiformes	55.88	66.0

the 8 included fossils to attach anywhere in the tree. The constraints enforced interfamilial relationships within all orders represented by more than two taxa (Anseriformes, Charadriiformes, Gruiformes) in addition to all applicable supraordinal relationships from three recent avian phylogenomic trees (Prum et al., 2015; Reddy et al., 2017; Kimball et al., 2019). All three analyses were performed using MrBayes v3.2.7a (Ronquist et al., 2012) under the $Mk+\Gamma$ substitution model and an $Exp(10)$ branch length prior. For each analysis, we ran 4 independent replicates, each with 4 Metropolis-coupled chains (three of which were incrementally heated) of 40 million generations. After discarding the first 40% of states as burn-in, we verified that the analyses reached convergence based on the ASDSF (<0.01), ESS values for scalar parameters (>200), and potential scale reduction factor (PSRF; ~ 1.00). Finally, we used the MRE consensus tree to summarize the post-burnin sample.

A long-recognized problem of node-dating analyses is the fact that fossil calibrations can only provide a reliable lower bound on the age of any given clade (Yang and Rannala, 2005; Benton and Donoghue, 2006; Wilkinson et al., 2010). To avoid arbitrary upper bounds, we used a simple Bayesian method devised by Hedman (2010) and first applied to fossil calibration design by Friedman et al. (2013). In this approach, the age of origin of a clade is informed by the sequence of the first appearance dates of its successive outgroups. The algorithm starts with the assumption that the age of the node connecting the most distant outgroup to the clade of interest is uniformly distributed between the first appearance of that outgroup and some arbitrary upper bound t_0 . The next outgroup diverges at a time that is uniformly distributed between its own first appearance date and the divergence time of the previous outgroup, integrating over the uncertainty in the latter. The process is then repeated until a non-uniform posterior distribution is obtained on the interval $[t_L, t_0]$, where t_L is the oldest known fossil belonging to the clade of interest (Hedman, 2010). Following Friedman et al. (2013), we took the conservative approach of excluding stratigraphically inconsistent outgroups (i.e., those that appear later in the fossil record despite diverging earlier). Together with the uncertain relationships within Neoaves (Jarvis et al., 2014; Prum et al., 2015; Suh, 2016) and the fact that few neornithine lineages predate the oldest known charadriiform records from the Paleocene/Eocene boundary (Mayr, 2014; Ksepka et al., 2017), this required extending the outgroup sequence into the neornithine stem group. We used recent phylogenies of Mesozoic birds to construct several alternative sequences (Appendix A). After setting $t_0 = 160$ Ma and evaluating the node age distributions at 1000 discrete time steps, we calculated the 95% credibility interval (CI) for the age of each calibrated node. We then averaged the 95% CI upper bounds across the different outgroup sequences to account for phylogenetic uncertainty, and used the resulting value as an upper bound for the corresponding calibration (Table 2).

2.7. Divergence time estimation

We used two independent approaches to infer charadriiform divergence times. First, we utilized the program MCMCTree from the PAML v4.9j suite (Yang, 2007) to carry out a two-step procedure involving the selection of the best-fit relaxed clock model, followed by the Bayesian inference of node ages on a fixed topology (set here to that of the total-evidence RAxML-NG tree after excluding the outgroup). MCMCTree provides a likelihood approximation method that offers significant speed-ups for large datasets (dos Reis and Yang, 2011), but does not implement models of morphological evolution. As a result, the divergence times of the 19 species sampled solely for morphological data were fully determined by the user-specified birth-death prior. Second, we used a penalized-likelihood rate-smoothing approach (Sanderson, 2002) implemented in treePL (Smith and O'Meara, 2012), which takes as its input one or more phylogenograms (trees with branch lengths in units of substitutions per site) and a set of calibrations specified as hard-bounded age ranges. The method makes no direct use of either

molecular or morphological character data, and is computationally inexpensive as a result, facilitating comparisons between different analytical choices and calibration sets. Below, we focus on the treePL framework; a detailed description of the MCMCTree analyses is provided in Appendix A.

Following the protocol of Maurin (2020), we first performed a “priming” analysis to choose the best settings for gradient-based, auto-differentiation-based, and autodifferentiation cross-validation-based optimizers. The analysis was performed using the full set of 14 calibrations listed in Table 2 and the total-evidence RAxML-NG tree stripped of the outgroup. Since treePL implements all calibrations as hard bounds (placing zero probability mass on ages outside the bounds), this effectively led to the truncation of calibrations 6, 12, and 13. Next, we performed the random subsample and replicate cross-validation procedure to determine the optimum value of the smoothing parameter. We tested for values ranging from 10^5 to 10^{-36} , with each new value 10 times smaller than the last ($cvmultstep = 0.1$), 10 random node removal iterations ($cviter$, default = 2), 10^9 cross-validation simulated annealing iterations ($cvsimaniter$, default = 5000) and with the thorough option enabled to ensure that the analysis iterates until convergence (Zaher et al., 2019). We repeated the procedure 5 times to test for the stability of the rate-smoothing value. Across the 5 runs, the estimates associated with the lowest chi-squared value spanned two orders of magnitude; for the following analyses, we used the median (10^{-9}), which was close to zero and thus allowed for relatively large differences in substitution rates among adjacent branches (Sanderson, 2002; Beaulieu and O'Meara, 2018). We performed sensitivity analyses under the values favored by the remaining four runs ($10^{-8}, 10^{-10}$), and found that they had little effect on the resulting node ages (Appendix A, Table A.4).

Preliminary analyses performed on the full calibration set revealed that the estimated root age always coincided with the upper bound placed on the corresponding calibration (Appendix A, Table A.4), suggesting that the rate-smoothing algorithm favored ages beyond the range we considered plausible. This behavior is known to be typical of treePL (Maurin, 2020) and has affected a large number of analyses performed using the method (Du et al., 2021; Wahlsteen et al., 2021; Roquet et al., 2022); as such, we did not interpret it as genuinely indicative of a Cretaceous crown age for the charadriiforms. To address this issue, we combined two previous protocols (Stein et al., 2018; Li et al., 2019) and repeated the analysis on each of the 1000 bootstrap pseudoreplicates generated for the total-evidence analysis. We used the R package rrriskDistributions (Belgorodski et al., 2017) to parameterize a lognormal root calibration density so as to satisfy the following constraints: to relax the upper bound, we placed 5% probability mass on ages exceeding 66.0 Ma. To account for uncertainty in the phylogenetic position of IGM 100/1435 (calibration 14), we averaged the posterior probability of its membership within the shorebird crown across the three analyses described in Section 2.6, and used the complement ($1 - \text{average PP} = 2.4\%$) as the probability mass to be placed on ages younger than the lower bound (55.88 Ma). For each bootstrap pseudoreplicate, the root age was then fixed to a random draw from the fitted distribution (log-scale mean = 4.1141, log-scale standard deviation = 0.0460) following Stein et al. (2018).

All 1000 analyses were performed under the previously found optimum smoothing value and optimization settings. Following Eberle et al. (2018), we increased the number of penalized-likelihood optimization iterations ($pliter = 10$, default = 2) and penalized-likelihood simulated annealing iterations ($plsimaniter = 10000$, default = 5000). The thorough option was used to ensure that the specified optimization routine converged. Every calibration other than calibration 14 was treated as a hard-bounded range assigned to the most recent common ancestor (MRCA) of a pair of anchor taxa. In the ML topology, this MRCA corresponded to the node listed in Table 2; however, this could not be guaranteed for the individual bootstrap pseudoreplicates, which

differed from the ML tree in topology as well as branch lengths. Finally, we used TreeAnnotator v2.6.6 (Bouckaert et al., 2019) to summarize the estimated divergence times as common-ancestor node heights. Using this method, the age of a given clade is averaged over the MRCA ages of the set of all taxa comprising that clade in the target tree (set here to the total-evidence ML tree), regardless of whether this set is monophyletic in a given tree or not (Heled and Bouckaert, 2013). In effect, this approach allowed us to incorporate a limited amount of calibration, topological, and branch length uncertainty into our divergence time estimates, which we quantified using 95% confidence intervals (CIs).

2.8. Macroevolutionary rate estimation

To infer the diversification dynamics of the Charadriiformes, we used Bayesian Analysis of Macroevolutionary Mixtures (BAMM) v2.6, a model-averaging approach that employs a time-scaled phylogeny to detect clade-specific shifts between distinct macroevolutionary regimes (Rabosky, 2014; Mitchell et al., 2018). The method relies on reversible-jump Markov chain Monte Carlo (rjMCMC) to sample models with different numbers of parameters, which correspond to within-regime rates of speciation and extinction. The number of regimes and the locations of the shifts between them are inferred from the data, and the estimates of macroevolutionary rates through time are marginalized over the models involving different regime numbers and shift configurations. After taxonomic reconciliation, 508 stratigraphically unique species-level fossil occurrences associated with the tips of the treePL time tree were located in the Paleobiology Database (<http://www.paleobiodb.org>; last accessed May 26, 2022) to inform the estimated extinction and fossil preservation rates (Mitchell et al., 2018).

We used the R package BAMMtools (Rabosky et al., 2014) to set the initial rate priors and the hyperprior on the exponential rate change parameter. The expected number of shifts was set to 1, and within-regime speciation rates were allowed to vary through time. The global sampling fraction was set to 0.903 (353 out of 391 shorebird species sampled in the tree). We performed two rjMCMC runs consisting of 4 Metropolis-coupled chains (one cold and three incrementally heated) of 50 million generations, sampling every 10,000 generations. After examining the posterior traces, the first 10% of samples were discarded as burnin, and convergence was assessed by calculating the ESS (> 200) and PSRF (< 1.01) using the R package coda (Plummer et al., 2006). We used BAMMtools to process the output, compare the prior and posterior probabilities of different diversification models, and calculate their Bayes factors relative to the best-supported model. Additionally, we computed the 95% credible set of rate shift configurations, and extracted the single maximum *a posteriori* (MAP) configuration. Finally, we summarized marginal macroevolutionary rates through time, calculated the mean rates inside and outside the shifted clades to determine the magnitude of each shift (Upham et al., 2021), and obtained the 95% credible intervals about the root and tip speciation rates within each regime to evaluate the support for rate variation over time.

3. Results

3.1. Data assembly and alignment

The final supermatrix obtained by concatenating all 27 loci (Table 1) included 28,531 sites from a single outgroup and 334 species of charadriiforms (Table S1), accounting for ~85% of the extant or recently extinct diversity (Dickinson and Remsen, 2013; Boyd, 2019; Clements et al., 2020). This concatenated alignment contained a total of 3,009,803 complete cells (excluding gaps and indeterminate residues), corresponding to 68.5% missing data. The number of loci per taxon (gene occupancy) ranged from 1 to all 27, with an average of 9.5 and a median of 6 (Appendix A, Fig. A.2). Every species was represented by at least 275 (white-eyed gull, *Ichthyaetus leucophthalmus*; Olrog's gull, *Larus atlanticus*; lava gull, *Leucophaeus fuliginosus*) and up to 26,852

(*Charadrius vociferus*) base pairs (average = 8984, median = 6063). The dataset included representatives of all 19 extant families, of which 5 monospecific (Dromadidae, Ibridorhynchidae, Pedionomidae, Pluvianellidae, Pluvianidae) and 7 multispecies (Chionidae, Haematopodidae, Jacanidae, Recurvirostridae, Rostratulidae, Stercorariidae, Thinocoridae) families were sampled exhaustively. The partial decisiveness of our concatenated alignment was 0.93, meaning that the subtrees induced by the incomplete taxon coverage of the individual genes uniquely define 93% of all possible trees when combined. The inclusion of morphological data increased the number of sampled charadriiform species to 353 (>90% of the extant or recently extinct diversity).

3.2. Gene tree analyses

In total, 34 sequences were excluded after the initial round of gene tree inference described in Section 2.2; the full list of the corresponding accession numbers and reasons for their removal are given in Appendix A (Table A.2). The final gene trees contained between 48 (BDNF, MUSK) and 312 (COI) tips (Table 1), with an average of 118 and a median of 95 tips per gene tree. On average, more species were included in the trees based on mitochondrial rather than nuclear loci (149 vs. 79 tips, respectively). Treating the entire mitochondrial genome as a single locus for the purposes of the DiscoVista analyses yielded a tree of 332 tips (including the outgroup).

Individual gene trees generally yielded high support for the monophyly of the three charadriiform suborders as well as the sister-group relationship of Scolopaci and Lari to the exclusion of Charadrii (Fig. 3). Gene tree discordance was nearly absent at the subordinal level except for the monophyly of Charadrii, which was weakly rejected by a single locus (MB2) that found Chionida alone to be the sister group of all shorebirds, albeit with virtually no bootstrap support (41%). Relationships within suborders were also in agreement with recent molecular phylogenies, and almost all of the “superfamily” or “parvorder”-level clades of Cracraft (2013) were strongly supported by 7–13 gene trees with little to no contradicting signal (Fig. 3). We found surprisingly ambiguous support for the monophyly of Alcoidea (Alcidae + Stercorariidae), which was weakly rejected by 7 nuclear genes (BDNF, CMOS, FGB7, MB2, MUSK, NTF3, and ODC). However, with the exception of FGB7, which yielded a poorly supported sister-group relationship between Laridae and Alcidae to the exclusion of Stercorariidae (bootstrap = 64%), this result was usually associated with a lack of reciprocal monophyly between Alcidae and Laridae, and with poor taxon sampling in the relevant region of the tree (Appendix A, Figs. A.9–A.10, A.18–A.19, A.27–A.28). Similarly, the higher-level relationships involving Dromadidae and Pluvianidae, two monotypic families with historically uncertain affinities, were subject to no appreciable gene tree conflict. Although the Egyptian plover (*Pluvianus aegyptius*) was only sampled for five of the analyzed genes (ADH, FGB7, GAPDH3–5, RAG1, and the mitogenome), these unanimously agreed on its sister-group relationship to the rest of Charadriida (Fig. 3). Similarly, the position of the crab plover (*Dromas ardeola*) as the sister taxon of coursers and pratincoles (Glareolidae) was only contradicted by a single gene (ADH), which instead lent moderate support to a clade uniting it with Laridae and Alcoidea (bootstrap = 73%).

3.3. Concatenated analyses

The average internode certainty (IC) value across the branches of the RAxML-NG tree was 0.63; of the 332 internal branches present in the unrooted tree, 9.6% had negative IC values (indicating that a conflicting bipartition had greater prevalence in the bootstrap set than the bipartition present in the maximum likelihood tree), and 88.6% had strictly positive internode certainties (indicating that the bipartition in the RAxML-NG tree occurred in the bootstrap set more frequently than any conflicting bipartition). Nearly all the branches associated with negative IC values represented internal relationships within species-rich genera

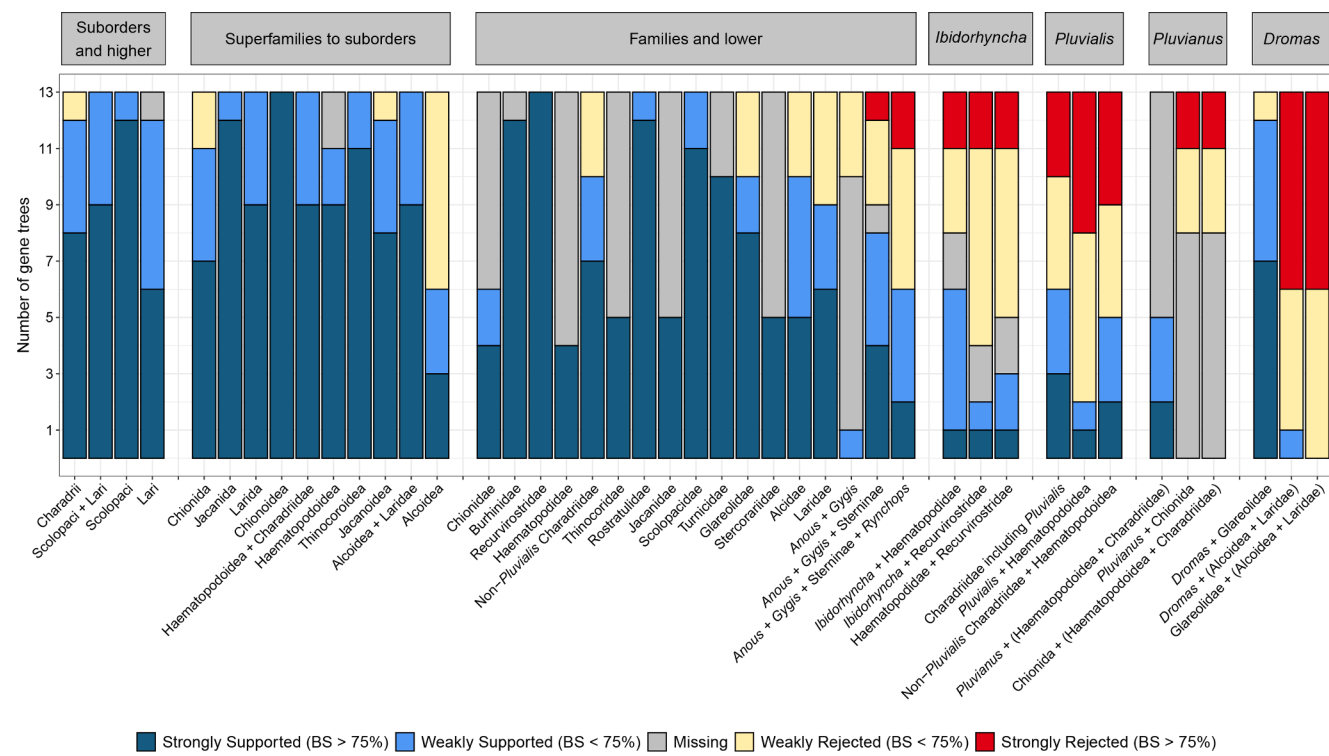


Fig. 3. Gene tree support for higher-level clades of shorebirds summarized using DiscoVista. Strong support or rejection are defined by the focal or conflicting clade exceeding a 75% bootstrap (BS) threshold, respectively; missing data refers to loci that lacked the taxon sampling needed to evaluate a given branch. For *Ibidorhyncha*, *Pluvialis*, *Pluvianus*, and *Dromas*, all three possible resolutions of the relevant branch have been scored.

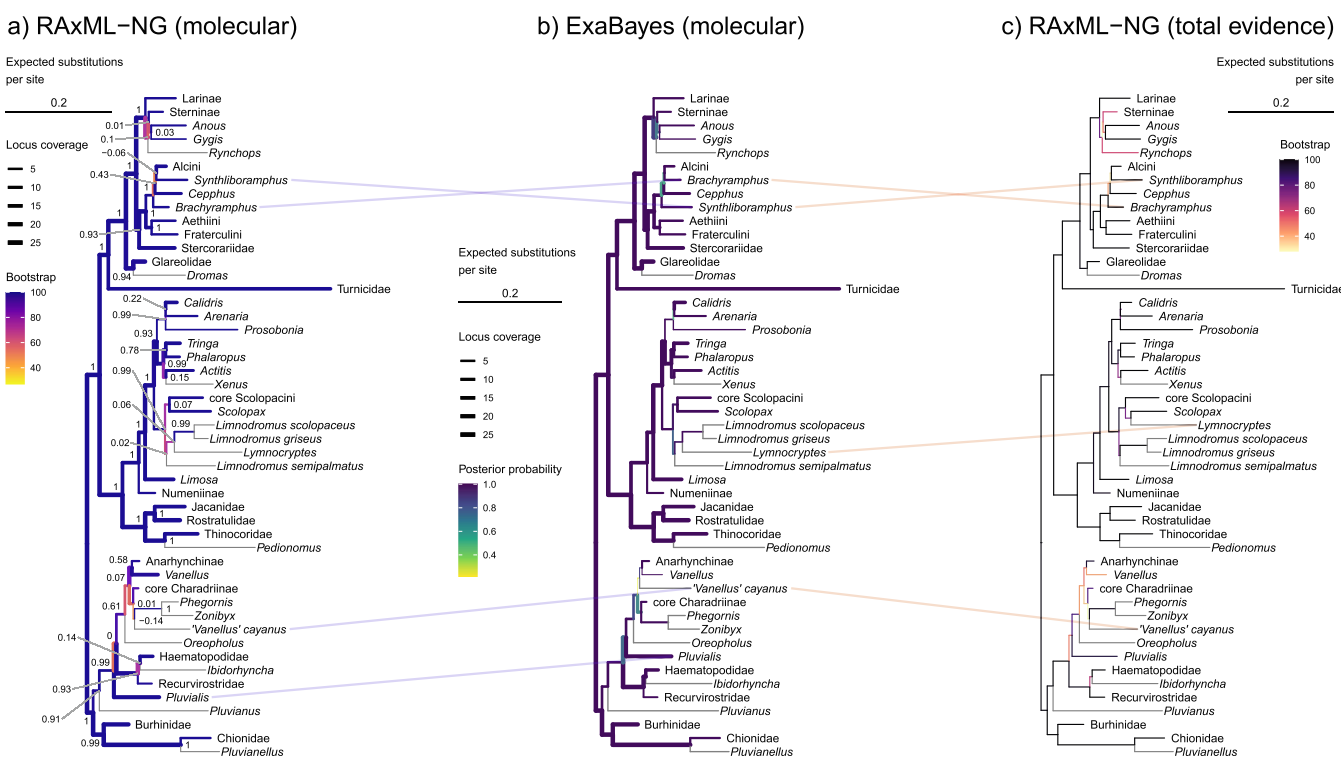


Fig. 4. Phylogenetic estimates for the Charadriiformes obtained from (a) concatenated maximum likelihood, (b) concatenated Bayesian, and (c) total-evidence maximum-likelihood analyses. Higher-level clades have been collapsed except when subject to topological conflict; branches subtending terminal taxa are shown in gray. The node labels of tree (a) denote internode certainty (IC) values; the light blue and red lines connect taxa with conflicting placements between a given pair of trees. Note that the per-branch locus coverage of the concatenation-based trees is calculated out of a total of 27 (mitochondrial loci analyzed separately). The full versions of all three trees are given in Appendix A (Figs. A.31–A.36).

such as *Calidris*, *Larus*, or *Vanellus*. The average bootstrap support (BS) across the RAxML-NG tree was 81%, with 72.9% of branches exceeding the threshold of BS = 70%. In contrast, the IC value exceeded by the same percentage of branches only amounted to 0.21. On average, the branches of the RAxML-NG tree were informed by 7.8 genes. Almost 88% of branches were informed by two or more loci, with 64% of branches represented by at least 5 loci. Using Bayesian correlation testing implemented in the R package bayestestR (Makowski et al., 2019), we found decisive evidence (*sensu* Kass and Raftery, 1995) that the locus coverage of a branch was positively correlated with both its internode uncertainty ($\rho = 0.25$, Bayes factor in favor of a nonzero $\rho = 5.79 \times 10^3$) and its bootstrap support ($\rho = 0.21$, Bayes factor = 3.14×10^2).

The average posterior probability (PP) on the ExaBayes tree was 0.89, with 76% of nodes exceeding the threshold of PP = 0.95. The average locus coverage of a branch in the ExaBayes tree was 7.6 genes, with 89% of branches informed by at least two loci and 64% of branches represented by 5 or more loci. Bayesian correlation analysis found decisive evidence for a relationship between the posterior probability of a branch and its locus coverage ($\rho = 0.22$, Bayes factor = 6.80×10^2). The average posterior probability of the 34 bipartitions present in the ExaBayes tree but not the RAxML-NG tree was 0.37, while the average bootstrap and internode certainty of the conflicting branches from the RAxML-NG tree amounted to 29% and -0.07 , respectively.

The RAxML-NG and ExaBayes analyses of the concatenated alignment agreed on all family-level relationships except the monophyly of the plovers (Fig. 4), which was weakly supported by Bayesian analysis (PP = 0.74) but not maximum likelihood. The latter method found *Pluvialis* outside of a poorly supported clade comprising all the remaining Charadriidae and Haematopodoidea (BS = 36%, IC = 0). The sister-group relationship between Haematopodidae and *Ibidorhyncha* was strongly supported by ExaBayes (PP = 0.99) but only weakly so by RAxML-NG (BS = 61%, IC = 0.14). Both analyses found strong support for the sister-group relationships between *Dromas* and Glareolidae (BS = 99%, IC = 0.94, PP = 1) and between *Pluvianus* and the rest of Charadriidae (BS = 99%, IC = 0.91, PP = 1). The two approaches also agreed on the interrelationships of the five major lineages of the Laridae, albeit with negligible support. Both analyses found a clade comprising the noddies (*Anous*) and white terns (*Gygis*) (BS = 46%, IC = 0.03, PP = 0.72) in a sister-group relationship with the true terns (Sterninae) (BS = 40%, IC = 0.01, PP = 0.7), with the resulting clade in turn forming the sister group of the skimmers (*Rynchops*) to the exclusion of the gulls (Larinae) (BS = 60%, IC = 0.10, PP = 0.87).

In contrast, among the auks, the interrelationships of *Brachyramphus*, *Synthliboramphus*, *Cephus*, and the true auks and murres (*Alca*, *Alle*, *Pinguinus*, *Uria*) differed between the two methods, though again with poor support values (BS < 50%, IC < 0, PP < 0.6) in both cases. Another notable intrafamilial conflict reflecting a near-total lack of resolution concerned the position of the pied plover ("Vanellus" *cayanus*), which was nested within Charadriinae in the maximum-likelihood tree (BS = 27%, IC = -0.14) but formed the sister group to a clade uniting all other lapwings (*Vanellus*) and Anarhynchinae in the ExaBayes tree (PP = 0.22). Aside from these limited conflicts, the two concatenation-based analyses yielded highly similar topologies, as evidenced by the fact that the RAxML-NG/ExaBayes Robinson-Foulds (RF; Robinson and Foulds, 1981) distance (0.102) was significantly smaller than the average distance between either of the two trees and 1000 sequence-only topologies from the Jetz et al. (2012) pseudoposterior (RAxML-NG: 0.352, 95% CI: 0.322–0.377; ExaBayes: 0.350, 95% CI: 0.322–0.377). To a lesser extent, this was also true for their distances from the supermatrix-based tree of Burleigh et al. (2015) (RAxML-NG = 0.297, ExaBayes = 0.305).

3.4. Combined analyses

The two trees generated by the evolutionary placement algorithm each differed from the total-evidence (TE) tree in the positions of 7 out of the 19 species without sequence data (Appendix A, Figs. A.35–A.36). Both rendered the lapwings (*Vanellus*) polyphyletic by allying the Senegal lapwing (*V. lugubris*) and the black-winged lapwing (*V. melanopterus*) with the tawny-throated dotterel (*Oreopholus*), while the TE analysis found a clade comprising the two species and the yellow-wattled lapwing (*V. malabaricus*) to form the sister group of all other lapwings (Fig. 6). However, only one of the nodes present in the TE tree but not the EPA trees received a bootstrap support value greater than 50% (average BS = 39.0%), and the same was true of most of the nodes connecting the morphology-only species to the rest of the tree (average BS = 54.6%). The TE/GT-EPA (0.097), TE/SSE-EPA (0.100), and GT-EPA/SSE-EPA (0.009) RF distances show that all three topologies are substantially closer to one another than to a sample of 1000 all-taxa trees from the Jetz et al. (2012) pseudoposterior (TE: 0.551, 95% CI: 0.518–0.578; GT-EPA: 0.549, 95% CI: 0.515–0.578; SSE-EPA: 0.550, 95% CI: 0.518–0.578). Given this high degree of congruence, none of the three trees was found to fit the combined data significantly better than the other two (Table 3).

When pruned down to the taxon sample of the concatenated trees, the TE tree differed from the ML topology in 23 nodes (RF distance = 0.069); however, these were generally poorly supported in both the concatenated ML tree (average BS = 29.2%, average IC = -0.06) and in the TE tree (average BS = 31.1%). The same was true of the concatenated Bayesian topology, from which the TE tree differed in 35 nodes (RF distance = 0.105) that generally exhibited low posterior probabilities in the former (average PP = 0.424) and low bootstrap values in the latter (average BS = 32.4%). Out of the 23 nodes present in the concatenated ML tree but not the TE tree, 17 were also absent from the concatenated Bayesian tree. Most prominent among these was a clade uniting Haematopodoidea with all plovers except *Pluvialis*, which was rejected by the Bayesian and TE trees in favor of a monophyletic Charadriidae (total-evidence BS = 47%). However, except for plover monophyly, higher-level relationships were nearly identical among the TE and concatenated trees (Fig. 4), with topological conflict largely restricted to intrageneric relationships within species-rich genera such as *Calidris*, *Larus*, or *Ochthodromus*. The only notable deviation from the sequence-only topologies involved the position of the jack snipe (*Lymnocryptes*), which was found within Limnodromini (and nested in the genus *Limnodromus*) in the concatenated trees (BS = 62%, IC = 0.06, PP = 0.96) but within Scolopacini (as the sister group of *Scolopax*) in the TE tree (BS = 74%).

3.5. Testing the positions of *Ibidorhyncha* and *Pluvialis*

Within the main supermatrix, the greatest amount of gene tree discordance underlay the relationship between the genus *Pluvialis* and

Table 3

Likelihood support for the total-evidence (TE) and group-together (GT-EPA) as well as split-scaffold-edges (SSE-EPA) evolutionary placement algorithm trees calculated from the combined dataset using IQ-TREE. Significance levels (p) and the inclusion in (+) or significant exclusion from (–) the 95% confidence set are given for the Kishino-Hasegawa (KH; Kishino and Hasegawa, 1989), Shimodaira-Hasegawa (SH; Shimodaira and Hasegawa, 1999), and approximately unbiased (AU; Shimodaira, 2002) tests; c (ELW) denotes confidence as measured using expected likelihood weight (Strimmer and Rambaut, 2002).

Tree	IQ-TREE log likelihood	p (KH)	p (SH)	p (AU)	c (ELW)
TE	−512510.587	0.739 +	1 +	0.742 +	0.730 +
GT-EPA	−512531.904	0.261 +	0.261 +	0.278 +	0.195 +
SSE-EPA	−512534.968	0.234 +	0.234 +	0.076 +	0.075 +

the remaining “core” plovers (Charadriidae), as well as the position of the ibisbill (*Ibidorhyncha*) relative to the oystercatchers (Haematopodidae) and stilts and avocets (Recurvirostridae) (Fig. 3). We therefore assembled an accessory dataset that included fewer taxa but many more sites to determine whether these conflicts can be resolved using a greater quantity of sequence data. However, the placement of both taxa continued to be subject to conflict between the ASTRAL species tree and the concatenated ML estimate, suggesting that the increase from 13 to 100 independent loci was insufficient to conclusively resolve their phylogenetic position (Fig. 5).

In contrast to the main analyses, which allied it with the oystercatchers (Fig. 3), the ibisbill emerged as the sister group of a (Haematopodidae + Recurvirostridae) clade in the multispecies coalescent tree (Fig. 5a), albeit with negligible support (localPP = 0.41). The quarter frequencies for the three alternative topologies around the branch of interest almost perfectly approached the $\frac{1}{3}$ ratio expected for a hard polytomy ($q_1 = 0.348$, $q_2 = 0.31$, $q_3 = 0.342$), and the polytomy test performed in ASTRAL failed to reject this hypothesis ($p = 0.882$). In the concatenated tree, the ibisbill formed the sister group to the Recurvirostridae alone (Fig. 5b), in contrast to both the main analysis and the multispecies coalescent tree. The resulting clade represented the most poorly supported node in the tree (BS = 56%), and was subtended by a near-zero-length branch.

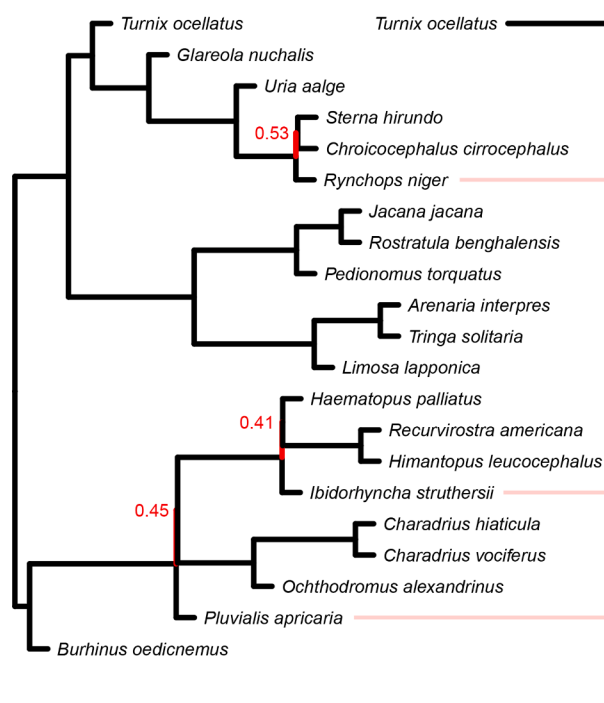
The 100-locus dataset was similarly inconclusive with respect to the monophyly of the plovers (Charadriidae), which received moderate support from the concatenated ML tree (BS = 74%; Fig. 5b) but was rejected by the ASTRAL species tree in favor of a poorly supported relationship between the core plovers and Haematopoidea (local PP = 0.45; Fig. 5a). The longer alignment therefore reproduced the same conflict observed in the analyses of the main supermatrix (Fig. 3). Here,

too, the quarter frequencies of alternative topologies were nearly uniformly distributed ($q_1 = 0.363$, $q_2 = 0.277$, $q_3 = 0.360$), failing to reject the null hypothesis that *Pluvialis*, the core plovers, and the Haematopoidea form a polytomy ($p = 0.491$).

3.6. Fossil calibrations

Our Bayesian re-analyses of the morphological matrix of Heingård et al. (2021) robustly supported a charadriiform affinity for specimen IGM 100/1435 from the Paleocene/Eocene boundary of Mongolia, which predates the previous oldest known remains of the clade (Fig. 1). Under all three topological constraints, IGM 100/1435 emerged as a crown-group charadriiform and specifically as a total-group member of the Chionoidea (average PP = 0.911; Appendix A, Fig. A.37), a position also supported by several partially constrained parsimony analyses of an earlier version of the same dataset (Musser and Clarke, 2020). For the purposes of calibration design, we took the conservative approach of associating the specimen with the least inclusive clade to which it could be assigned with a PP ≥ 0.95 , a condition satisfied only by the entire charadriiform crown group (Table 2). When constructing the outlier sequences, which require taxa to be associated with branches rather than nodes, the fossil was treated as *incertae sedis* within the total group of Charadrii. The analyses also weakly (average PP = 0.528) but consistently placed SMF Av 619, another early Eocene fossil (Fig. 1), within the total group of Larida. However, the least inclusive node to which the specimen could be assigned with a PP ≥ 0.95 was again the charadriiform crown group, rendering it redundant as a potential calibration.

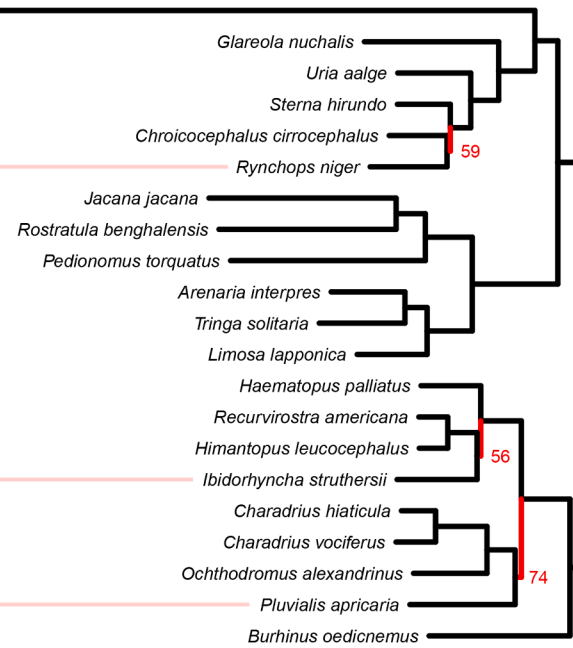
a) Multispecies coalescent



Coalescent units (non-terminal branches only)

1

b) Concatenated, maximum likelihood



Expected substitutions per site

0.05

Fig. 5. Phylogenetic estimates for the Charadriiformes obtained from the (a) multispecies coalescent and (b) concatenated maximum-likelihood analyses of the 100-locus dataset designed to test the phylogenetic position of *Ibidorhyncha* and *Pluvialis*. Node labels denote (a) local posterior probabilities (localPP) and (b) bootstrap support (BS); unlabeled nodes received support of 1.0 localPP and 100% BS. Red branches and light red lines highlight taxa with conflicting placements.

3.7. Divergence time estimation

Our MCMCTree analyses failed to converge, as indicated by low ESS

(<200) and high PSRF (>1.05) values for a number of node ages. We therefore refer to the treePL results instead, with the exception of the age of the charadriiform crown, which was assumed rather than estimated in

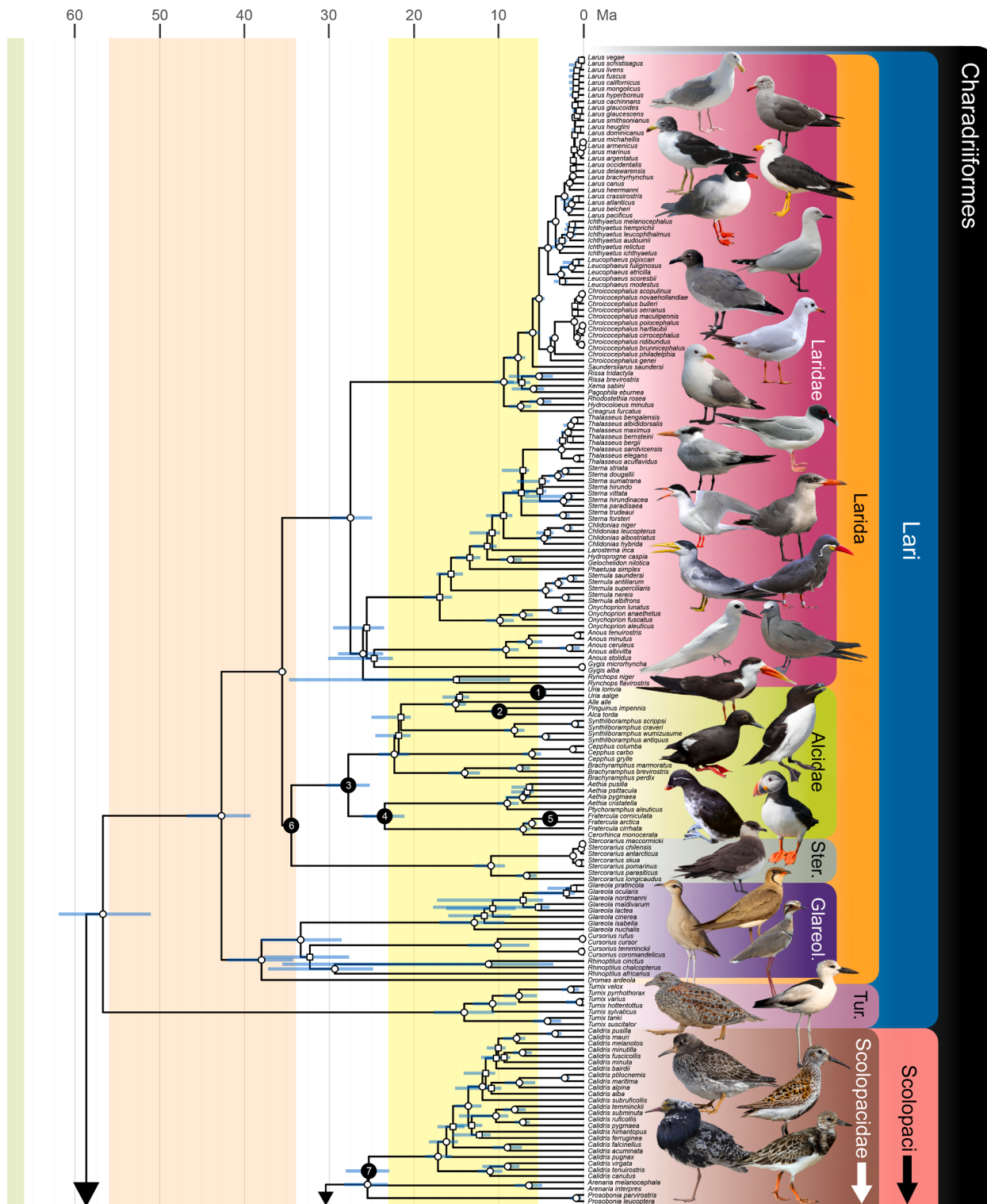


Fig. 6. Time-calibrated phylogeny of 353 species of shorebirds based on the penalized-likelihood rate-smoothing analysis of a total-evidence phylogram inferred using RAxML-NG from 27 genes and 69 morphological characters. The figure and this caption continue on the opposite page. Nodes with bootstrap support $\geq 70\%$ are indicated by circles; nodes with bootstrap support $< 70\%$ are indicated by squares. Fossil-calibrated nodes are shown in black and numbered as in Table 2. Blue bars denote 95% confidence intervals based on 1000 bootstrap pseudoreplicates. Shaded tabs represent higher-level clades; background shading indicates geochronological epochs. Ma = million years ago; Ster. = Stercorariidae; Glareol. = Glareolidae; Tur. = Turnicidae; Jac. = Jacanidae; Haem. = Haematopodidae; Rec. = Recurvirostridae; Bur. = Burhinidae; Chion. = Chionidae; LC = Late Cretaceous; Pal = Paleocene; Eo = Eocene; Ol = Oligocene; Mio = Miocene; Pli = Pliocene; Ple = Pleistocene. Representative species are illustrated next to their lineages; see Appendix A (Table A.5) for full image credits.

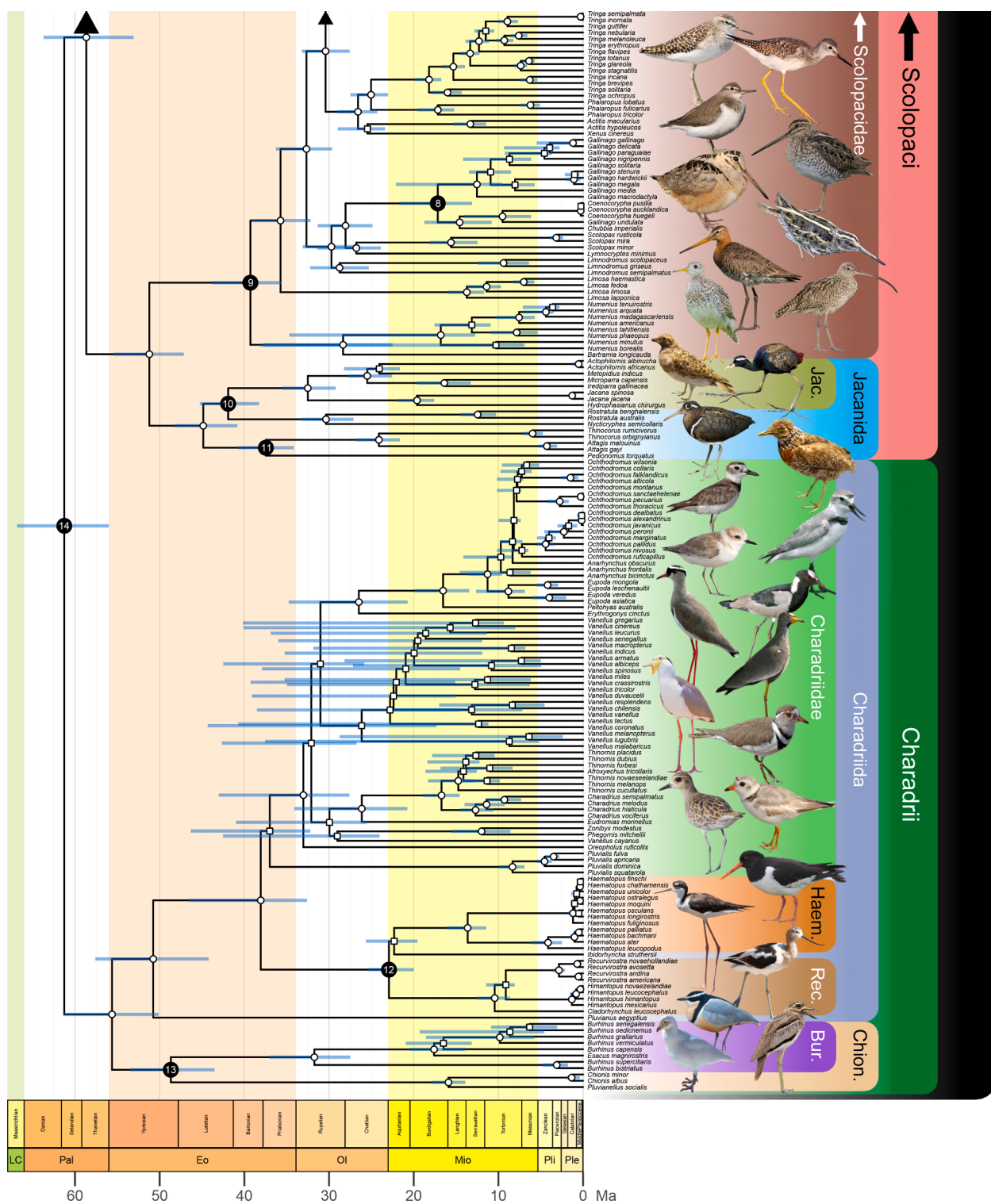


Fig. 6. (continued).

the treePL analysis (see Section 2.7). The MCMCTree estimates of this parameter reached moderate (>100) to high (>200) effective sample sizes in two out of the four runs performed; however, the combined ESS values were low (<100) due to large amounts of within-chain variation in the remaining two runs. The among-chain variation was substantial but tolerable ($\text{PSRF} = 1.069$), reflecting the fact that all four MCMCTree runs were sampling broadly similar root ages (range of within-chain means: 56.7–58.2 Ma; combined mean: 57.6 Ma). In all cases, the posterior mean shifted toward the present compared to the mean of the

user-specified prior (61.1 Ma). These results indicate a highly imprecise but consistent dating of the origin of crown-group charadriiforms to the late Paleocene. Importantly, none of the corresponding 95% highest posterior density intervals (calculated either from the individual runs or from the combined sample) extended into the Cretaceous, whereas all extended into the earliest Eocene, slightly beyond the soft lower bound specified by calibration 14 (Table 2). This result suggests that the root age prior chosen for the treePL analyses was plausible, and should not bias the remaining node ages.

The treePL time tree shows Eocene mean stem ages for most (14 out of 19) of the shorebird families, indicating an early period of steady diversification (Fig. 6). The estimated timeline suggests that the current diversity of the second and third most species-rich shorebird families (Scolopacidae: 97 species, Charadriidae: 68 species) has been accumulated over long periods of time, as the confidence intervals of their crown ages were concentrated in the Eocene (Scolopacidae: 95% CI = 35.6–43.8 Ma; Charadriidae: 95% CI = 31.1–45.2 Ma), substantially predating those of the other families. In contrast, the most diverse charadriiform family, Laridae (107 species), is notably younger (24.9–29.8 Ma), and its subfamilies did not start diversifying until the middle Miocene.

The precision of non-root divergence time estimates was moderate in both absolute (average 95% CI width = 5.31 Ma) and relative terms (average 95% CI width relative to the mean = 0.713), indicating modest success at accommodating the uncertainty contained in the source phylogenograms. Precision was considerably higher for the 13 calibrated nodes whose ages were freely estimated (absolute: 4.99 Ma, relative: 0.205) than for the uncalibrated nodes (absolute: 5.32 Ma, relative: 0.732). On average, the 95% CIs on the ages of the calibrated nodes were much narrower than their specified calibration ranges (median shrinkage factor = 7.24); the ratio was smallest for calibration 8 (2.60) and greatest for calibration 6. The latter calibration, assigned to the (Alcidae + Stercorariidae) clade (Table 2), constituted a clear outlier whose 95% CI was entirely concentrated at the lower bound of the specified range, indicating a conflict between the available fossil evidence and the branch lengths of the analyzed phylogenograms. A similar problem also affected calibration 5, whose 95% CI was likewise tightly distributed around the user-specified minimum. Most of the remaining outliers in terms of node age precision involved the sister-group relationships of taxa that were only sampled for morphological data; this was the case for 95% CIs that were both unusually narrow and unusually wide. Many of the latter were concentrated in the lapwing clade (genus *Vanellus*; Fig. 6), which contained 10 of the 19 morphology-only taxa included in our analysis (Appendix A, Figs. A.35–A.36).

3.8. Macroevolutionary rate estimation

The maximum *a posteriori* (MAP) rate shift configuration (PP = 0.127) on the treePL time tree included two well-supported rate shifts, associated with (1) the clade comprising the gull genera *Larus*, *Ichthyaetus*, *Leucophaeus*, and *Chroicocephalus*, and (2) the clade uniting the Old World oystercatchers (*Haematopus fuliginosus* + *Haematopus finschi*) (Fig. 7a). Given the large number of nearly equiprobable rate shift configurations included in the 95% credible set, we also examined the maximum shift credibility (MSC) configuration, which contained the same two shifts. A shift subtending either node (1) or the node immediately above it appeared in 501 out of the 506 configurations included in the 95% credibility set (cumulative PP = 0.95), while a shift subtending node (2) was present in 423 of these configurations (cumulative PP = 0.90). Relative to the background regime excluding both of the shifted clades, the model-averaged time-weighted mean rate of the (*Larus* + *Chroicocephalus*) clade was accelerated by a factor of 8.8 for speciation and 8.1 for net diversification; for the Old World *Haematopus* clade, these ratios amounted to 10.4 and 8.4, respectively. The elevated net diversification rates were nearly constant through time for both the gulls (root 95% CI: 0.427–0.905 sp·Myr⁻¹, tip 95% CI: 0.445–0.883 sp·Myr⁻¹) and the oystercatchers (root 95% CI: 0.068–1.614 sp·Myr⁻¹, tip 95% CI: 0.073–1.608 sp·Myr⁻¹), whereas the background regime exhibited gradually declining diversification with a slight uptick in the last 5 Myr (root 95% CI: 0.044–0.150 sp·Myr⁻¹, tip 95% CI: 0.069–0.104 sp·Myr⁻¹) (Fig. 7b).

The rate increases associated with the (*Larus* + *Chroicocephalus*) clade and Old World oystercatchers represented the only shifts present in the MAP and MSC configurations that were sampled significantly more often than expected under the prior alone (marginal odds ratio >

5). The total number of shifts was generally greater, as the posterior probability of models involving 3 (PP = 0.31), 4 (PP = 0.26), and 5 (PP = 0.16) shifts exceeded that of the 2-shift models (PP = 0.15). The Bayes factor of the best supported, 5-shift model relative to the 2-shift model amounted to 8.21, indicating positive evidence in favor of the former (Kass and Raftery, 1995). After the shifts among the derived larines and at the (*H. fuliginosus* + *H. finschi*) node, the next most often sampled transition to a new rate regime occurred within the skuas (*Stercorarius*), receiving support from 188 of the configurations included in the 95% credibility set (cumulative PP = 0.23).

4. Discussion

4.1. Congruence and conflict in higher-level charadriiform relationships

The topologies inferred by our concatenated and total-evidence analyses are broadly consistent with previous estimates based on molecular data (Ericson et al., 2003; Paton et al., 2003; Paton and Baker, 2006; Baker et al., 2007; Fain and Houde, 2007; Hackett et al., 2008; Prum et al., 2015; Hu et al., 2017). Our results support the three-suborder division of the Charadriiformes into Charadrii, Scolopaci, and Lari; the position of the morphologically aberrant buttonquails (Turnicidae) as the earliest-diverging lineage within the Lari; and most of the previously proposed interfamilial relationships (Baker et al., 2007; Burleigh et al., 2015; Prum et al., 2015). In conjunction with previous work, these findings indicate that most of the higher-order charadriiform relationships are robustly resolved. However, several localized areas of uncertainty persist despite the comprehensive taxon sampling employed here.

Our analyses failed to resolve the question of whether the typical plovers (Charadriidae) are monophyletic (Baker et al., 2012; Hu et al., 2017) or paraphyletic with respect to Haematopodidae (Ericson et al., 2003; Baker et al., 2007; Fain and Houde, 2007; Burleigh et al., 2015). We found the branch in question to be associated with the most extensive gene tree discordance of all the relationships we examined (Fig. 3), and this phenomenon persisted even in the expanded, 100-locus dataset (Fig. 5), which showed nearly equal support for all three possible interrelationships between *Pluvialis*, core Charadriidae, and Haematopodidae. These results strongly suggest that, contrary to the conclusion derived by Baker et al. (2012) from a much smaller dataset, the observed discordance is due to incomplete lineage sorting across two successive speciation events rather than mere stochastic error. Similarly, we find no evidence that mitochondrial loci are especially prone to inferring plover paraphyly because of their high mutational variance (Baker et al., 2012), as the mitochondrial loci analyzed in this study supported charadriid monophyly when concatenated (BS = 81%), in contrast to the ambiguous results from nuclear genes. Our results suggest that resolving the problem of plover monophyly will require dedicated species-tree analyses sampling thousands of loci, well beyond the scope of this study. The same conclusion also applies to the phylogenetic position of the ibisbill (*Ibidorhyncha*) vis-à-vis the oystercatchers (Haematopodidae) and avocets and stilts (Recurvirostridae), which also remained ambiguous even after expanding our locus sampling to 100 nuclear genes (Fig. 5). As a result, the recent taxonomic suggestion to reduce Ibidorhynchidae to a subfamily of oystercatchers (Cracraft, 2013) should be viewed as premature, and the possibility that the base of Haematopodidae forms a hard polytomy cannot be ruled out at present.

Our study helps indicate directions for future research by identifying other regions of the shorebird tree that could not be confidently resolved using the relatively small number of loci employed here. One such area of uncertainty represents the interrelationships of the four major lineages comprising the true auks (Alcinae): the guillemots (*Cephus*), brachyramphine murrelets (*Brachyramphus*), synthliboramphine murrelets (*Synthliboramphus*), and the tribe Alcini, which unites the extant razorbills (*Alca*), dovekies (*Alle*), and murres (*Uria*) with the recently extinct great auk (*Pinguinus*). The interrelationships of these clades have so far proved elusive (Strauch, 1985; Moum et al., 1994; Friesen et al., 1996;

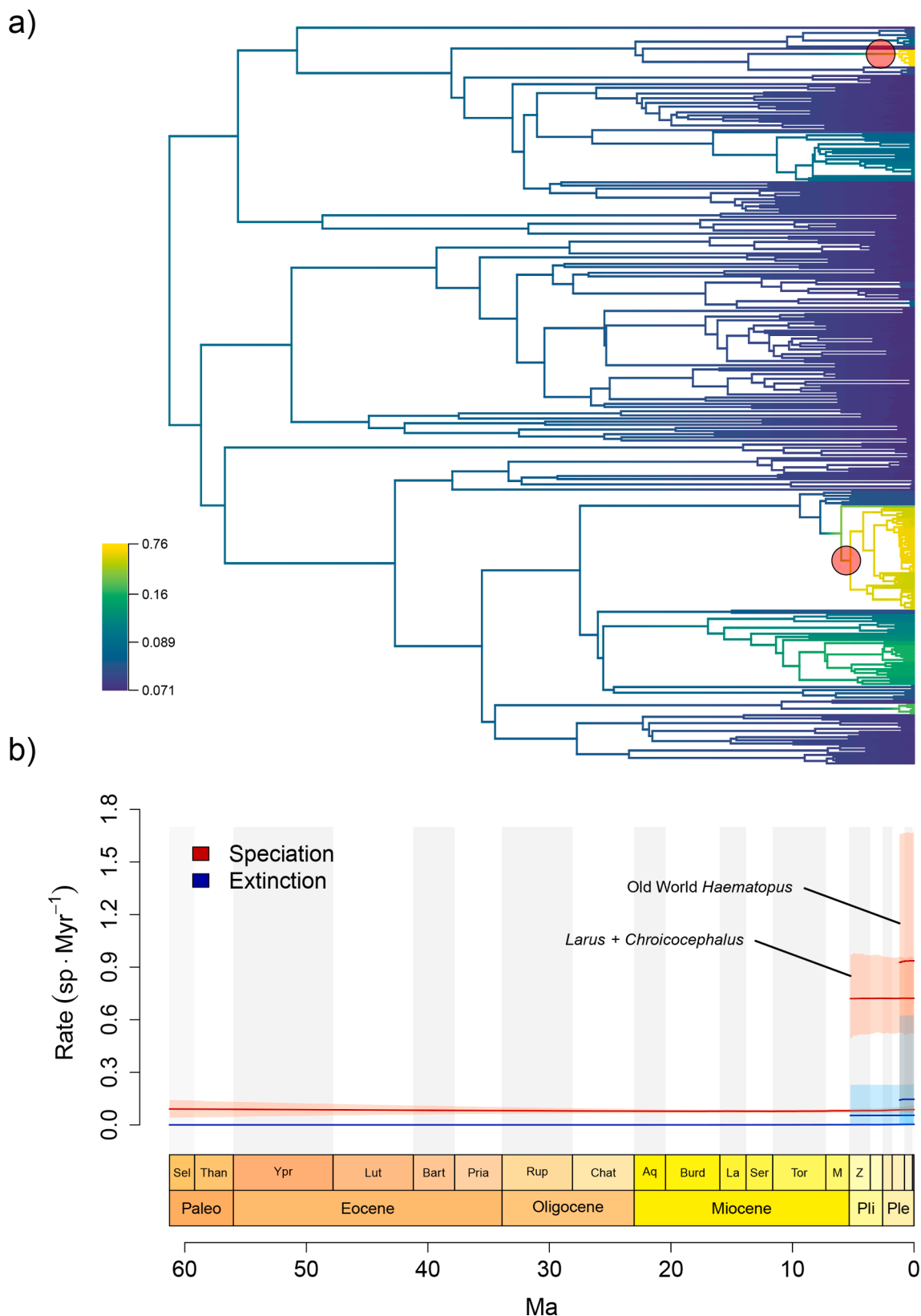


Fig. 7. Top: phylograte plot for the treePL time tree, with branches colored by the net diversification rate (in $\text{sp} \cdot \text{Myr}^{-1}$) and rate shifts denoted by red circles (a). Bottom: corresponding rate-through-time (RTT) plot showing the mean speciation and extinction rates for each rate regime, along with their associated 95% credibility intervals (b).

Baker et al., 2007; Burleigh et al., 2015; Smith and Clarke, 2015), and could not be resolved using our data (Fig. 4). This uncertainty is expected given the combination of very short internodes connecting the four taxa and the relatively long branches subtending them, a feature characteristic of ancient rapid radiations (Lanyon, 1988; Whitfield and Lockhart, 2007). Indeed, our dating analysis suggests that the three speciation events giving rise to the lineages in question took place within a time span of just 0.8 Myr (Fig. 6). A comparably rapid sequence of successive divergences also characterizes the interrelationships of the five major lineages of the Laridae, often classified as separate subfamilies (Cracraft, 2013; Boyd, 2019): the gulls (Larinae), true terns (Sterninae), skimmers (*Rynchops*), noddies (*Anous*), and white terns (*Gygis*). Interestingly, although the analyses of our main supermatrix yielded consistent results (Fig. 4) that also agreed with the phylogenetic tree of Prum et al. (2015) in grouping the skimmers and true terns to the exclusion of the gulls, this was not the case for the taxon-poor 100-locus alignment derived from Prum et al., 2015's (Prum et al., 2015) data, where concatenated and species-tree analyses contradicted each other as well as the main supermatrix (Fig. 5). This disagreement indicates that in order to resolve the early stages of the larid radiation, extensive sampling of both species and loci will be necessary as a means for resolving the short internodes and breaking up the branches subtending the five subfamilies.

Finally, topological conflict also occurs among the sandpipers (Scolopacidae), especially with regard to the position of the jack snipe (*Lymnocryptes*; Fig. 4), for which little sequence data is currently available. As a result, the sister-group relationship between the jack snipe and woodcocks (*Scolopax*) inferred by our total-evidence analysis may represent the only case in which the molecular topology was overturned by a strong signal in Strauch, 1978's (Strauch, 1978) morphological data, since a (*Lymnocryptes* + *Scolopacini*) clade is conspicuously present in the morphology-only tree (Appendix A, Fig. A.30) and exhibits a long branch indicative of a high number of shared apomorphies. Additional sequence data will be required to test this morphology-based hypothesis against the previously suggested alternative of a sister-group relationship between the jack snipe and dowitchers (*Limnodromus*) (Baker et al., 2007).

Despite maximizing taxon sampling based on the available molecular and morphological data, our study still contains gaps in taxonomic coverage that suggest where additional sampling effort should be directed. Of the 13 charadriiform families comprising more than one species, the buttonquails (Turnicidae) had the lowest coverage in the present study (7 out of 17 species), and currently available sequence data do not even make it possible to test whether *Turnix* is monophyletic with respect to the monotypic *Ortyxelos*. We suggest that sequencing the latter genus as well as additional *Turnix* species should be a priority for future studies seeking to improve taxon sampling within the Charadriiformes.

4.2. Taxonomic implications

While the higher-level phylogeny of shorebirds is generally well-established, the comprehensive taxon sampling of our study helps reveal instances of nonmonophly at the genus level. These may represent genuine conflicts between phylogenetic relationships and established taxonomy that have gone undetected by earlier molecular analyses with limited taxon sampling. However, it is also possible that at least some of these cases reflect the relatively low number of loci available to inform shallow divergences (stochastic error), or phenomena such as introgressive hybridization and persistence of ancestral polymorphisms across a rapid succession of speciation events (systematic error). Accordingly, our taxonomic recommendations primarily focus on ensuring genus-level monophly under multiple phylogenetic hypotheses put forward both here and in previous studies.

Our analyses yield a scolopacid topology that is generally similar to the phylogeny of Gibson and Baker (2012), as expected given our

reliance on much of the same sequence data. Accordingly, our findings are consistent with the changes implemented by recent taxonomies in response to the latter study, including the expansion of the genera *Calidris* and *Tringa* to ensure their monophly (Dickinson and Remsen, 2013; Boyd, 2019; Clements et al., 2020), and the reassignment of the imperial snipe to a separate genus (*Chubbia*) to preserve the monophly of *Gallinago* (Boyd, 2019). However, our results suggest that the disintegration of the genus *Gallinago* initiated by Gibson and Baker (2012) may proceed even further as taxon sampling continues to improve, since we find the giant snipe ("Gallinago" *undulata*) to be more closely related to *Coenocorypha* and *Chubbia* than to the rest of the genus. While recovered consistently and with high statistical support (RAxML-NG BS/IC = 94%/0.68, ExaBayes PP = 1, TE BS = 89%), this relationship is for now only supported by the single locus for which "G." *undulata* is sampled (COI); we were able to confirm that it persists regardless of which of the giant snipe COI sequences currently available from BOLD (Ratnasingham and Hebert, 2007) is used. Given that the result is based on just one gene, we refrain from advocating for immediate generic reassignment, but note that if corroborated by analyses with broader locus sampling, it may require resurrecting the genus *Homoptilura* Gray, 1840 for the giant snipe to maintain generic monophly.

The narrow concept of the genus *Charadrius* and the reassignment of most of its former species to the resurrected genera *Afroxyechus*, *Eupoda*, and *Ochthodromus*, as well as the expansion of the pre-existing genera *Anarhynchus* and *Thinornis*, was adopted by the taxonomy employed here (Boyd, 2019) to reflect recent phylogenetic findings (Barth et al., 2013; Dos Remedios et al., 2015), but is only partially compatible with our own results. We corroborate previous findings (Barth et al., 2013; Burleigh et al., 2015; Dos Remedios et al., 2015) showing that most of the species traditionally assigned to *Charadrius* are more closely related to *Anarhynchus*, *Erythrogonyx*, and the Vanellinae than to the type (*C. hiaticula*), thus violating the monophly of the genus and of the subfamily Charadriinae as traditionally conceived (Cracraft, 2013). We also find the wrybill (*Anarhynchus frontalis*) to be deeply nested within the clade consisting of most of the former *Charadrius* species ("CRD II" sensu Dos Remedios et al., 2015; Anarhynchinae sensu Boyd, 2019). Within this clade, the Caspian plover (*Eupoda asiatica*), greater sandplover (*E. leschenaultii*), lesser sand-plover (*E. mongala*), and the oriental plover (*E. veredus*) form a well-supported clade (RAxML-NG BS/IC = 82%/0.47, ExaBayes PP = 0.98, TE BS = 83%) corresponding to Boyd, 2019's (Boyd, 2019) genus *Eupoda*, which represents an early-diverging lineage that branches off immediately after the red-kneed dotterel (*Erythrogonyx*) and the inland dotterel (*Peltorhynchus*) (Fig. 6).

In contrast, the relationships among the derived anarhynchines that form the sister group of *Eupoda* are less clear, and we find no support for the reciprocal monophly of the genera *Anarhynchus* and *Ochthodromus* sensu Boyd (2019). Following Barth et al. (2013) and Dos Remedios et al. (2015), the former genus was supposed to unite the wrybill with the double-banded plover ("Charadrius" *bicinctus*) and the New Zealand plover ("Charadrius" *obscurus*). Our concatenated and total-evidence ML analyses find negligible support for a sister-group relationship between *A. frontalis* and "C." *bicinctus* (BS/IC = 32%/-0.01, TE BS = 34%), with "C." *obscurus* as the sister group to *Ochthodromus* (BS/IC = 37%/0, TE BS = 42%), whose monophly likewise received virtually no support (BS/IC = 22%/0, TE BS = 22%). Conversely, the ExaBayes tree finds *A. frontalis* alone as the sister group to *Ochthodromus* and nests a poorly supported ("C." *bicinctus* + "C." *obscurus*) clade (PP = 0.75) deep within the latter genus as the sister group to the red-capped plover (*O. ruficapillus*), also with negligible support (PP = 0.59). A detailed examination of gene tree support reveals that of the five loci that recovered the monophly of (*A. frontalis* + "C." *bicinctus*) in the analyses of Dos Remedios et al. (2015, Fig. 2), only three (ADH, COI, ND3) continue to do so here (Appendix A, Figs. A.5, A.11, A.22). In contrast, while a clade uniting all three putative species of *Anarhynchus* was not present in any of the six gene trees of Dos Remedios et al. (2015, Fig. 2), despite receiving maximum possible support (PP = 1) in their

concatenated analysis, our ADH and COI phylogenies do recover such a group. These differences between the gene tree estimates obtained here and by Dos Remedios et al. (2015) may be due to analytical approach (ML vs. Bayesian inference), sampling scheme (single vs. multiple individuals per species), or taxonomic scope (all shorebirds vs. paraphyletic assemblage of non-vanelline charadriids). To safeguard generic monophyly under all plausible hypotheses, we suggest combining the genera *Anarhynchus* and *Ochthodromus*, in which case *Anarhynchus* Quoy and Gaimard, 1832 takes the priority. The subfamily Anarhynchinae would then comprise the genera *Anarhynchus*, *Erythrogonyx*, and *Peltohyas*, which are universally recognized by major taxonomies (Dickinson and Remsen, 2013; Boyd, 2019; Clements et al., 2020), as well as the genus *Eupoda* (*sensu* Boyd, 2019), whose monophyly is robustly and consistently supported by recent analyses.

The second major assemblage of the former *Charadrius* species ("CRD I" *sensu* Dos Remedios et al., 2015; Charadriinae *sensu* Boyd, 2019) is rendered paraphyletic by the inclusion of the genera *Thinornis* and *Afroxyechus*. Like Barth et al. (2013) and Dos Remedios et al. (2015), we find that the former genus is itself nonmonophyletic, as its two traditionally accepted species (*T. novaeseelandiae* and *T. cucullatus*) span a clade that also includes three plovers usually assigned to *Charadrius* (the little ringed plover, "C." *dubius*; Forbes's plover, "C." *forbesi*; and the long-billed plover, "C." *placidus*) as well as the black-fronted dotterel, occasionally placed in its own separate genus ("Elseyornis" *melanops*). These results therefore support the expansion of *Thinornis* following Boyd (2019). Moreover, we find the three-banded plover ("Afroxyechus" *tricollaris*) to be nested within the expanded *Thinornis* as well, contrasting with the results of Dos Remedios et al. (2015) who found it outside the (*Charadrius* + *Thinornis*) clade. The latter result was extremely weakly supported (PP = 0.47) and only appeared in the concatenated analysis despite its absence from any of the individual gene trees, whereas we find strong support for the inclusion of "A." *tricollaris* within *Thinornis* (RAxML-NG BS/IC = 75%/0.52, ExaBayes PP = 0.99, TE BS = 70%), a position also favored by 5 out of the 6 gene trees of Dos Remedios et al. (2015). We therefore suggest that the species be reassigned to the latter genus as a new combination, *Thinornis tricollaris*.

Our final recommendation concerns the pied plover ("Vanellus" *cayanus*), whose affinity to lapwings (*Vanellus*) is rejected by our analyses (Fig. 4). Instead, we variously recover it as the sister group to an early-diverging charadriine clade comprising the diademed sandpiper-plover (*Phegornis*) and the rufous-chested plover (*Zonibyx*) in the concatenation-based and total-evidence maximum-likelihood trees (BS/IC = 27%/-0.14; TE BS = 29%), or to the (*Vanellinae* + *Anarhynchinae*) clade in the ExaBayes tree (PP = 0.22). Both positions have no appreciable support, and further contradict the COI gene tree (the only locus for which the pied plover is sampled; Appendix A, Fig. A.11), which finds it to be the earliest-diverging member of *Vanellus*, as well as the tree inferred from Strauch, 1978's (Strauch, 1978) morphological data (Appendix A, Fig. A.30), which allies it with *Phegornis* and "*Afroxyechus*". To account for this range of hypotheses, we propose to resurrect the genus *Hoploxypterus* Bonaparte, 1856 for the species.

4.3. A new timeline for charadriiform evolution

Despite wall-clock run times of more than 80 days, our MCMCTree node-dating analyses failed to reach convergence, suggesting that the size of our tree (353 tips) may be close to the upper limit at which Bayesian divergence time estimation remains feasible without consortium-scale computational resources. The modest effective sample size for the root age parameter did not allow us to constrain the origin of the charadriiform crown beyond the mid- to late Paleocene, in agreement with the recent phylogenomic study of Kuhl et al. (2020). Such a dating is consistent with an explosive radiation of neoavian lineages in the wake of the end-Cretaceous mass extinction (Ericson et al., 2006; Suh, 2016; Berv and Field, 2017), and (unlike the early mitogenomic timescales; Paton et al., 2002; Pereira and Baker, 2006; Baker et al.,

2007) does not require positing a long period during which the clade supposedly diversified but failed to leave behind a fossil record. Indeed, our MCMCTree results, while imprecise, lend no support to a Cretaceous origin of shorebirds, despite relying on a root calibration that was designed to allow for this possibility. At the same time, our age estimates for the charadriiform crown are slightly older than the early Eocene dates favored by many earlier studies (Smith, 2011: 53.6 Ma; Claramunt and Cracraft, 2015: 53.5 Ma; Prum et al., 2015: 48.8–50.6 Ma; Smith and Clarke, 2015: 49.3 Ma; cf. Fig. 1). These earlier estimates contradict the recent evidence for the crown-charadriiform affinities of fossil specimens from the early Eocene of Virginia (SMF Av 619; Mayr, 2016) and the Paleocene–Eocene boundary of Mongolia (IGM 100/1435; Hood et al., 2019), which received support from the phylogenetic analyses of Musser and Clarke (2020) and Heingård et al. (2021), as well as our own re-analyses of the dataset employed by the latter study.

While our re-analyses of the Heingård et al. (2021) character matrix found weak but consistent support for the placement of SMF Av 619 and IGM 100/1435 within the total groups of Larida and Chionoidea, respectively, only the former phylogenetic position is compatible with our divergence time estimates. Our treePL point estimate for the age of the Larida/Turnicidae split (56.7 Ma) exceeds the age of SMF Av 619 (54.17–53.7 Ma based on calcareous nannoplankton zonation; Anthoniissen and Ogg, 2012; Mayr, 2016), which lies well within the corresponding 95% confidence interval (51.0–61.9 Ma). In contrast, our dating of the Chionoidea/Burhinidae divergence (48.7 Ma) is substantially younger than the estimated age of IGM 100/1435 (~55.88 Ma; see Appendix A), which even falls outside the relevant 95% CI (43.5–53.5 Ma). Should more evidence emerge for a deeply nested phylogenetic position of this fossil, the timescale presented here would have to be altered by shifting the root age even deeper into the past, and/or by positing a more rapid succession of interfamilial divergences.

Our timescale diverges somewhat from recent phylogenomic studies with respect to the age of individual charadriiform subclades. Compared to the pseudoposterior of Jetz et al. (2012), our treePL common-ancestor ages were so young as to be excluded from the 95% pseudoposterior CIs for Charadriidae (37.0 Ma vs. 37.5–59.2 Ma) and Recurvirostridae (10.4 Ma vs. 13.8–27.4 Ma). For Larida and a number of its constituent subclades (Alcidae, Alcoidea, Glareoloidea, Laridae), the difference was even more pronounced but opposite in direction, as we found these taxa to be significantly older than suggested by the Jetz et al. (2012) time tree distribution. Not only their means but also their entire 95% CIs fell outside of those derived from the Jetz et al. (2012) pseudoposterior, which produced a mean age for the Alcidae that was almost 50% younger than the common-ancestor mean age yielded by our treePL analysis (16.0 vs 27.7 Ma). Our estimates for the ages of Alcoidea, the (Alcoidea + Laridae) clade, and Larida also exceed those of other recent analyses (Claramunt and Cracraft, 2015; Prum et al., 2015; Kuhl et al., 2020), although they are not as old as suggested by early studies that relied on obsolete calibrations (Pereira and Baker, 2008).

The difference can be largely attributed to our use of calibration 6 (Table 2), representing a late Eocene pan-alcid of uncertain affinities whose position within the clade was nevertheless supported by a formal phylogenetic analysis (Smith, 2011). The post-Eocene dates suggested for the Alcidae/Stercorariidae divergence (or even more inclusive clades) by recent studies may thus exemplify the "zombie lineage" problem described by Springer et al. (2017), in which molecular divergence times turn out to be younger than the known fossil record allows. The same underestimation of divergence times was recently reported for the Gruiformes by Musser et al. (2019), and may be relatively widespread as a result of efforts to correct for the implausibly old divergences yielded by earlier studies by means of overly stringent calibration choice. Conversely, the criteria employed here that allowed calibration 6 to be used could be criticized as too lax given the fragmentary nature of the material and the long temporal gap separating it from the next oldest pan-alcid occurrence. To assess its impact on the node ages within Larida, we conducted an additional treePL analysis in

which we stripped calibration 6 of its lower bound. The resulting time tree suggested substantially younger ages for Alcoidea (29.8 vs. 34.4 Ma) as well as its immediate child (Alcidae; 24.4 vs 27.7 Ma) and parent (Alcoidea + Laridae; 32.5 vs. 35.6 Ma) nodes; in all these cases, the new point estimate fell outside the 95% CI around the original value ([Appendix A](#), Table A.4). However, this effect already became insignificant at the level of Larida (40.1 vs 42.7 Ma), indicating that the relatively low amount of rate smoothing employed in our analysis localized the impact of any given calibration to a small part of the tree. Removal of the lower bound from the deeply nested calibration 5, which likewise prevented treePL from sampling younger ages for the corresponding divergence, had even less of an appreciable effect on the remaining divergence times ([Appendix A](#), Table A.4).

Unlike Bayesian node dating, which can rely on a birth–death branching-process prior in the absence of informative data, treePL merely time-scales a previously inferred phylogram, and its results necessarily reflect the limitations of the data from which the phylogram was inferred. In our analysis, this was evident in the highly precise and implausibly young ages inferred for the divergences between the cream-colored courser (*Cursor cursor*) and Burchell's courser (*Cursor rufus*) (0.004–0.01 Ma), and between Temminck's courser (*Cursor temminckii*) and the Indian courser (*Cursor coromandelicus*) (0.004–0.467 Ma). In both cases, the second member of the pair was only represented in the combined matrix by morphological data, and its codings were indistinguishable from those of its sister group. This induced near-zero-length branches in the total-evidence phylogram, which could only be accounted for by means of near-zero divergence times ([Fig. 6](#)). At the same time, morphology-only taxa were relatively free to move across the tree in the bootstrap analysis, since the 69 morphological characters contributed little to the overall tree likelihood, and as such incurred only a negligible likelihood penalty upon separating these taxa from their close relatives. Their stem ages were consequently averaged across both shallow and deep divergences, resulting in very low precision. This problem is exemplified by the node uniting the yellow-wattled, Senegal, and black-winged lapwing (*Vanellus malabaricus* + *V. melanopterus*), three taxa sampled exclusively for morphological data. As a result, the corresponding divergence was associated with the widest 95% confidence interval observed in our tree (0.004–32.3 Ma; [Fig. 6](#)).

4.4. Tempo and mode of shorebird diversification

Our BAMM analysis of shorebird macroevolutionary dynamics shows that a clade comprising 4 genera of gulls (including a total of 49 species) entered a new diversification regime characterized by accelerated rates of speciation and extinction that have not appreciably declined since the clade's origin. This scenario is consistent with the findings of [Jetz et al. \(2012\)](#), who identified a gull clade of similar composition and size (44 species) as the single fastest-diversifying group of extant birds. Their estimate of the gull net diversification rate (0.74 sp·Myr⁻¹) falls well within the 95% credibility interval obtained in this study (0.44–0.87 sp·Myr⁻¹), further confirming a large degree of congruence between the two analyses. In contrast, we were unable to corroborate [Jetz et al. \(2012\)](#)'s ([Jetz et al., 2012](#)) inference of a diversification shift at the origin of the (Alcoidea + Laridae) clade, which we found to be much older (35.6 vs. 21.1 Ma); note that this difference is reduced but still present even after removing the lower bound from calibration 6 ([Appendix A](#), Table A.4). Conversely, our BAMM analysis lends support to an additional rate shift associated with a clade comprising 8 species of Old World oystercatchers, which was not detected by [Jetz et al. \(2012\)](#). However, our inference of an extremely rapid radiation for this clade is consistent with the high degree of ecomorphological similarity and incomplete reproductive barriers among its constituent species ([Senfeld et al., 2020](#)). Both factors have in fact rendered species delimitation problematic within the group, suggesting that the support for the shift and its inferred magnitude may decrease if several proposed synonymies (e.g., of *Haematopus finschi* or *H. osculans* with *H. ostralegus*; [Senfeld](#)

[et al., 2020](#)) were to be recognized and reduced the total diversity of the clade.

5. Conclusions

The densely sampled, time-calibrated, total-evidence tree of shorebirds presented here is a major step toward understanding the evolution of one of the most ecomorphologically diverse and species-rich clades of non-passerine birds. It represents a substantial advance over earlier studies that were not consistent with the fossil record of the group, did not include as many species, or only did so without informing their placement by character data. We expect that the availability of a generally well-resolved phylogeny accounting for over nine tenths of the extant diversity of the clade will greatly facilitate future comparative, biogeographical, and macroecological studies of shorebirds. In addition to highlighting areas of robust support, which span most of the suprafamilial backbone of the charadriiform tree, we also identify regions of persisting uncertainty to be prioritized by future analyses with increased taxon and locus sampling. Our study demonstrates the difficulties intrinsic to estimating a large, comprehensively sampled time tree from a sparse molecular supermatrix, and presents a protocol that can be readily applied to other clades posing similar challenges.

Funding

This research did not receive any specific grant from funding agencies in the public, commercial, or not-for-profit sectors.

Data accessibility

All GenBank accession numbers, alignments, tree files, configuration files, and R scripts are available from the Dryad Digital Repository: <https://doi.org/10.5061/dryad.xksn02vjc>.

CRediT authorship contribution statement

David Černý: Conceptualization, Methodology, Formal analysis, Writing – original draft, Writing – review & editing, Visualization. **Rosy Natale:** Conceptualization, Data curation, Writing – original draft, Writing – review & editing, Visualization.

Declaration of Competing Interest

The authors declare that they have no known competing financial interests or personal relationships that could have appeared to influence the work reported in this paper.

Acknowledgments

We thank two anonymous reviewers for their suggestions and insight, and to John Bates and Graham Slater for valuable comments on early drafts of the manuscript. We are grateful to Mario dos Reis, Siavash Mirarab, and Alexis Stamatakis for their help with the methods and software used in this study, and to Natalie Dos Remedios, Josephine D'Urban Jackson, Miriam Heingård, Simon Ho, and Grace Musser for kindly sharing their data with us. The quality of our sequence data was greatly improved by comments from John Boyd and Laurent Raty, to whom we are indebted for their attention to detail. We further thank the wildlife photographers whose work features in this paper for making their art available under Creative Commons licenses, and Susan Kidwell for sharing stratigraphic information relevant to calibration design. Large-scale analyses were performed on the Midway2 Research Computing Cluster at the University of Chicago; we are also indebted to Graham Slater for access to additional computing resources.

Appendix A. Supplementary material

Supplementary data associated with this article can be found, in the online version, at <https://doi.org/10.1016/j.ympev.2022.107620>.

References

- Aberer, A.J., Kober, K., Stamatakis, A., 2014. ExaBayes: massively parallel Bayesian tree inference for the whole-genome era. *Mol. Biol. Evol.* 31 (10), 2553–2556.
- Agnarsson, I., May-Collado, L.J., 2008. The phylogeny of Cetartiodactyla: The importance of dense taxon sampling, missing data, and the remarkable promise of cytochrome *b* to provide reliable species-level phylogenies. *Mol. Phylogenetic Evol.* 48 (3), 964–985.
- Almalki, M., Ismail, M., Gaber, A., 2021. The efficacy of COI barcoding and ISSR markers in molecular identification of diverse bird *Sturnula saundersi* populations along the Red Sea coast, Kingdom of Saudi Arabia. *J. Env. Biol.* 42, 24–32.
- Anthonissen, D.E., Ogg, J.G., 2012. Cenozoic and Cretaceous biochronology of planktonic foraminifera and calcareous nannofossils. In: Gradstein, F.M., Ogg, J.G., Schmitz, M.D., Ogg, G.M. (Eds.), *The Geologic Time Scale 2012*. Elsevier, Boston, MA, pp. 1083–1127.
- Baker, A.J., Pereira, S.L., Paton, T.A., 2007. Phylogenetic relationships and divergence times of Charadriiformes genera: multigene evidence for the Cretaceous origin of at least 14 clades of shorebirds. *Biol. Lett.* 3 (2), 205–210.
- Baker, A.J., Yatsenko, Y., Tavares, E.S., 2012. Eight independent nuclear genes support monophyly of the plovers: The role of mutational variance in gene trees. *Mol. Phylogenetic Evol.* 65 (2), 631–641.
- Barbosa, A., Moreno, E., 1999. Evolution of foraging strategies in shorebirds: An ecomorphological approach. *Auk* 116 (3), 712–725.
- Barth, J.M.I., Matschiner, M., Robertson, B.C., 2013. Phylogenetic position and subspecies divergence of the endangered New Zealand Dotterel (*Charadrius obscurus*). *PLOS ONE* 8 (10), e78068.
- Beaulieu, J.M., O'Meara, B.C., 2018. Can we build it? Yes we can, but should we use it? Assessing the quality and value of a very large phylogeny of campanulid angiosperms. *Am. J. Bot.* 105 (3), 417–432.
- Belgorodski, N., Greiner, M., Tolksdorf, K., Schueler, K., 2017. rriskDistributions: fitting distributions to given data or known quantiles. R package vol 2.1.2. Available from <https://cran.r-project.org/package=rriskDistributions>. Accessed May 30, 2022.
- Benson, D.A., Cavanaugh, M., Clark, K., Karsch-Mizrachi, I., Ostell, J., Pruitt, K.D., Sayers, E.W., 2017. GenBank. *Nucl. Acids Res.* 46 (D1), D41–D47.
- Benton, M.J., Donoghue, P.C.J., 2006. Paleontological evidence to date the tree of life. *Mol. Biol. Evol.* 24 (1), 26–53.
- Berger, S.A., Stamatakis, A., 2010. Accuracy of morphology-based phylogenetic fossil placement under maximum likelihood. In: *ACS/IEEE International Conference on Computer Systems and Applications – AICCSA 2010*, pp. 1–9.
- Berger, S.A., Stamatakis, A., Lücking, R., 2011. Morphology-based phylogenetic binning of the lichen genera *Graphis* and *Allographa* (Ascomycota: Graphidaceae) using molecular site weight calibration. *Taxon* 60 (5), 1450–1457.
- Berv, J.S., Field, D.J., 2017. Genomic signature of an avian Lilliput Effect across the K-Pg extinction. *Syst. Biol.* 67 (1), 1–13.
- Bininda-Emonds, O.R.P., 2014. An introduction to supertree construction (and partitioned phylogenetic analyses) with a view toward the distinction between gene trees and species trees. In: Garamszegi, L.Z. (Ed.), *Modern Phylogenetic Comparative Methods and Their Application in Evolutionary Biology: Concepts and Practice*, chapter 3. Springer-Verlag, Berlin, Germany, pp. 49–76.
- Björklund, M., 1994. Phylogenetic relationships among Charadriiformes: Reanalysis of previous data. *Auk* 111 (4), 825–832.
- Bonaparte, C.L., 1856. Excursions dans les divers musées d'Allemagne, de Hollande et de Belgique, et Tableaux parallèles de l'ordre des Échassiers. *Compt. Rend. Hebd. Séances Acad. Sci.* 43, 410–421.
- Bouckaert, R., Vaughan, T.G., Barido-Sottani, J., Duchêne, S., Fournier, M., Gavryushkina, A., Heled, J., Jones, G., Kühnert, D., De Maio, N., Matschiner, M., Mendes, F.K., Müller, N.F., Ogilvie, H.A., du Plessis, L., Popinga, A., Rambaut, A., Rasmussen, D., Siveroni, I., Suchard, M.A., Wu, C.-H., Xie, D., Zhang, C., Stadler, T., Drummond, A.J., 2019. BEAST 2.5: An advanced software platform for Bayesian evolutionary analysis. *PLOS Comput. Biol.* 15 (4), e1006650.
- Boyd, J.H., 2019. Taxonomy in Flux: Version 3.05, August 2, 2019. <http://jboyd.net/Taxo/List.html>. Accessed September 29, 2020.
- Bravo, G.A., Schmitt, C.J., Edwards, S.V., 2021. What have we learned from the first 500 avian genomes? *Ann. Rev. Ecol. Evol. Syst.* 52 (1), 611–639.
- Bridge, E.S., Jones, A.W., Baker, A.J., 2005. A phylogenetic framework for the terns (Sternini) inferred from mtDNA sequences: implications for taxonomy and plumage evolution. *Mol. Phylogenetic Evol.* 35 (2), 459–469.
- Brodkorb, P., 1967. Catalogue of fossil birds: part 3 (Ralliformes, Ichthyornithiformes. Charadriiformes). *Bull. Florida State Mus., Biol. Sci.* 11 (3), 99–220.
- Brown, C., Ward, D., 1990. The morphology of the syrinx in the Charadriiformes (Aves): Possible phylogenetic implications. *Bonn. zool. Beitr.* 41 (2), 95–107.
- Brown, J.W., Payne, R.B., Mindell, D.P., 2007. Nuclear DNA does not reconcile 'rocks' and 'clocks' in Neoaves: a comment on Ericson et al. *Biol. Lett.* 3 (3), 257–260.
- Brown, J.W., Rest, J.S., García-Moreno, J., Sorenson, M.D., Mindell, D.P., 2008. Strong mitochondrial DNA support for a Cretaceous origin of modern avian lineages. *BMC Biol.* 6 (1), 6.
- Brown, J.W., van Tuinen, M., 2011. Evolving perceptions on the antiquity of the modern avian tree. In: Dyke, G.J., Kaiser, G. (Eds.), *Living Dinosaurs: The Evolutionary History of Modern Birds*. John Wiley & Sons, London, UK, pp. 306–324.
- Burleigh, J.G., Kimball, R.T., Braun, E.L., 2015. Building the avian tree of life using a large-scale, sparse supermatrix. *Mol. Phylogenetic Evol.* 84, 53–63.
- Chen, W., Zhang, C., Pan, T., Liu, W., Li, K., Hu, C., Chang, Q., 2018. The mitochondrial genome of the Kentish Plover *Charadrius alexandrinus* (Charadriiformes: Charadriidae) and phylogenetic analysis of Charadrii. *Genes Genom.* 40 (9), 955–963.
- Chesser, R.T., Billerman, S.M., Burns, K.J., Cicero, C., Dunn, J.L., Hernández-Baños, B.E., Kratter, A.W., Lovette, I.J., Mason, N.A., Rasmussen, P.C., Remsen, J.V., Stotz, D.F., Winker, K., 2021. Sixty-second supplement to the American Ornithological Society's Check-list of North American Birds. *Ornithology* 138 (3), ukab037.
- Chesser, R.T., Billerman, S.M., Burns, K.J., Cicero, C., Dunn, J.L., Kratter, A.W., Lovette, I.J., Mason, N.A., Rasmussen, P.C., Remsen, J.V., Stotz, D.F., Winker, K., 2020. Sixty-first supplement to the American Ornithological Society's Check-list of North American Birds. *Auk* 137 (3), ukaa030.
- Chu, P.C., 1995. Phylogenetic reanalysis of Strauch's osteological data set for the Charadriiformes. *Condor* 97 (1), 174–196.
- Chu, P.C., 1998. A phylogeny of the gulls (Aves: Larinae) inferred from osteological and integumentary characters. *Cladistics* 14 (1), 1–43.
- Chu, P.C., Eisenschenk, S.K., Zhu, S.-T., 2009. Skeletal morphology and the phylogeny of skuas (Aves: Charadriiformes, Stercorariidae). *Zool. J. Linn. Soc.* 157 (3), 612–621.
- Claramunt, S., Cracraft, J., 2015. A new time tree reveals Earth history's imprint on the evolution of modern birds. *Sci. Adv.* 1 (11), e1501005.
- Clements, J.F., Schulenberg, T.S., Illiff, M.J., Billerman, S.M., Fredericks, T.A., Sullivan, B.L., Wood, C.L., 2019. The eBird/Clements checklist of birds of the world: v2019. <http://www.birds.cornell.edu/clementschecklist/download>. Accessed September 29, 2020.
- Cohen, B.L., Baker, A.J., Blechschmidt, K., Dittmann, D.L., Furness, R.W., Gerwin, J.A., Helbig, A.J., de Korte, J., Marshall, H.D., Palma, R.L., Peter, H.-U., Ramli, R., Siebold, I., Willcox, M.S., Wilson, R.H., Zink, R.M., 1997. Enigmatic phylogeny of skuas (Aves: Stercorariidae). *Proc. R. Soc. Lond. B* 264 (1379), 181–190.
- Collar, N.J., Donald, P.F., Kirwan, G.M., 2021. Species, subspecies or morph—what was the Canary Islands Oystercatcher? *Ibis* 163 (4), 1500–1505.
- Cracraft, J., 1981. Toward a phylogenetic classification of the recent birds of the world (Class Aves). *Auk* 98 (4), 681–714.
- Cracraft, J., 2013. Avian higher-level relationships and classification: Nonpasseriforms. In: Dickinson, E.C., Remsen, J.V. (Eds.), *The Howard and Moore Complete Checklist of the Birds of the World, Volume 1: Non-passerines* (4th edition). Aves Press, Eastbourne, UK, pp. xxi–xlii.
- Cracraft, J., Barker, F.K., Braun, M., Harshman, J., Dyke, G.J., Feinstein, J., Stanley, S., Cibois, A., Schikler, P., Beresford, P., García-Moreno, J., Sorenson, M.D., Yuri, T., Mindell, D.P., 2004. Phylogenetic relationships among modern birds (Neornithes): toward an avian tree of life. In: Cracraft, J., Donoghue, M.J. (Eds.), *Assembling the Tree of Life*. Oxford University Press, New York, pp. 468–489.
- Cracraft, J., Houde, P., Ho, S.Y.W., Mindell, D.P., Fjeldså, J., Lindow, B., Edwards, S.V., Rahbek, C., Mirarab, S., Warnow, T., Gilbert, M.T.P., Zhang, G., Braun, E.L., Jarvis, E.D., 2015. Response to Comment on "Whole-genome analyses resolve early branches in the tree of life of modern birds". *Science* 349 (6255), 1460b.
- Crochet, P.-A., Bonhomme, F., Lebreton, J.-D., 2000. Molecular phylogeny and plumage evolution in gulls (Larini). *J. Evol. Biol.* 13 (1), 47–57.
- Czech, L., Barbera, P., Stamatakis, A., 2020. Genesis and Gappa: processing, analyzing and visualizing phylogenetic (placement) data. *Bioinform.* 36 (10), 3263–3265.
- De Pietri, V.L., Worthy, T.H., Scofield, R.P., Cole, T.L., Wood, J.R., Mitchell, K.J., Cibois, A., Jansen, J.J.F.J., Cooper, A.J., Feng, S., Chen, W., Tennyson, A.J.D., Wragg, G.M., 2020. A new extinct species of Polynesian sandpiper (Charadriiformes: Scopoliidae: *Prosobonia*) from Henderson Island, Pitcairn Group, and the phylogenetic relationships of Prosobonia. *Zool. J. Linn. Soc.* 192 (4), 1045–1070.
- Dickinson, E.C., Remsen, J.V., 2013. The Howard and Moore Complete Checklist of the Birds of the World, Volume 1: Non-passerines (4th edition). Aves Press, Eastbourne, UK.
- dos Reis, M., Yang, Z., 2011. Approximate likelihood calculation on a phylogeny for Bayesian estimation of divergence times. *Mol. Biol. Evol.* 28 (7), 2161–2172.
- Dos Remedios, N., Lee, P.L.M., Burke, T., Székely, T., Küpper, C., 2015. North or south? Phylogenetic and biogeographic origins of a globally distributed avian clade. *Mol. Phylogenetic Evol.* 89, 151–159.
- Dove, C.J., 2000. A descriptive and phylogenetic analysis of plumulaceous feather characters in Charadriiformes. *Ornithol. Monogr.* 51, 1–163.
- Doyle, J.J., 2022. Defining coalescent genes: theory meets practice in organelle phylogenomics. *Syst. Biol.* 71 (2), 476–489.
- Du, X.-Y., Lu, J.-M., Zhang, L.-B., Wen, J., Kuo, L.-Y., Mynssen, C.M., Schneider, H., Li, D.-Z., 2021. Simultaneous diversification of Polypodiidae and angiosperms in the Mesozoic. *Cladistics* 37 (5), 518–539.
- Dufour, P., Guerra Carande, J., Renaud, J., Renoult, J.P., Lavergne, S., Crochet, P.-A., 2020. Plumage colouration in gulls responds to their non-breeding climatic niche. *Global Ecol. Biogeogr.* 29 (10), 1704–1715.
- D'Urban Jackson, J., Zefania, S., Moehy, S., Bamford, A.J., Bruford, M.W., Székely, T., 2019. Ecology, conservation, and phylogenetic position of the Madagascar Jacana *Actophilornis albinucha*. *Ostrich* 90 (4), 315–326.
- Eberle, J., Dimitrov, D., Valdez-Mondragón, A., Huber, B.A., 2018. Microhabitat change drives diversification in pholcid spiders. *BMC Evol. Biol.* 18 (1), 141.
- Edgar, R.C., 2004. MUSCLE: multiple sequence alignment with high accuracy and high throughput. *Nucl. Acids Res.* 32 (5), 1792–1797.
- Ericson, P.G.P., Anderson, C.L., Britton, T., Elzánowski, A., Johansson, U.S., Källersjö, M., Ohlson, J.I., Parsons, T.J., Zucon, D., Mayr, G., 2006. Diversification of Neovaves: integration of molecular sequence data and fossils. *Biol. Lett.* 2 (4), 543–547.

- Ericson, P.G.P., Envall, I., Irestedt, M., Norman, J.A., 2003. Inter-familial relationships of the shorebirds (Aves: Charadriiformes) based on nuclear DNA sequence data. *BMC Evol. Biol.* 3 (1), 16.
- Fain, M.G., Houde, P., 2004. Parallel radiations in the primary clades of birds. *Evolution* 58 (11), 2558–2573.
- Fain, M.G., Houde, P., 2007. Multilocus perspectives on the monophyly and phylogeny of the order Charadriiformes (Aves). *BMC Evol. Biol.* 7 (1), 35.
- Faircloth, B.C., 2015. PHYLUCE is a software package for the analysis of conserved genomic loci. *Bioinform.* 32 (5), 786–788.
- Feng, S., Stiller, J., Deng, Y., Armstrong, J., Fang, Q., Reeve, A.H., Xie, D., Chen, G., Guo, C., Faircloth, B.C., Petersen, B., Wang, Z., Zhou, Q., Diekhans, M., Chen, W., Andreu-Sánchez, S., Margaryan, A., Howard, J.T., Parent, C., Pacheco, G., Sinding, M.-H.S., Puetz, L., Cavill, E., Ribeiro, A.M., Eckhart, L., Fjeldså, J., Hosner, P.A., Brumfield, R.T., Christidis, L., Bertelsen, M.F., Sicheritz-Ponten, T., Tietze, D.T., Robertson, B.C., Song, G., Borgia, G., Claramunt, S., Lovette, I.J., Cowen, S.J., Njoroge, P., Dumbacher, J.P., Ryder, O.A., Fuchs, J., Bunce, M., Burt, D.W., Cracraft, J., Meng, G., Hackett, S.J., Ryan, P.G., Jónsson, K.A., Jamieson, I.G., da Fonseca, R.R., Braun, E.L., Houde, P., Mirarab, S., Suh, A., Hansson, B., Ponnikas, S., Sigeman, H., Stervander, M., Frandsen, P.B., van der Zwan, H., van der Sluis, R., Visser, C., Balakrishnan, C.N., Clark, A.G., Fitzpatrick, J.W., Bowman, R., Chen, N., Cloutier, A., Sackton, T.B., Edwards, S.V., Foote, D.J., Shakya, S.B., Sheldon, F.H., Vignal, A., Soares, A.R., Shapiro, B., González-Solís, J., Ferrer-Obiol, J., Rozas, J., Riutort, M., Tigano, A., Friesen, V., Dalén, L., Urrutia, A.O., Székely, T., Liu, Y., Campana, M.G., Corvelo, A., Fleischer, R.C., Rutherford, K.M., Gemmell, N.J., Dussex, N., Mouritsen, H., Thiéle, N., Delmore, K., Lievdogel, M., Franke, A., Hoeppner, M.P., Krone, O., Fudickar, A.M., Milá, B., Ketterson, E.D., Fidler, A.E., Friis, G., Parody-Merino, Á.M., Battley, P.F., Cox, M.P., Lima, N.C.B., Prosdocimi, F., Parchman, T.L., Schlinger, B.A., Loiselle, B.A., Blake, J.G., Lim, H.C., Day, L.B., Fuxjager, M.J., Baldwin, M.W., Braun, M.J., Wirthlin, M., Dikow, R.B., Ryder, T.B., Camenisch, G., Keller, L.F., DaCosta, J.M., Hauber, M.E., Louder, M.I.M., Witt, C.C., McGuire, J.A., Mudge, J., Megna, L.C., Carling, M.D., Wang, B., Taylor, S.A., Del-Rio, G., Aleixo, A., Vasconcelos, A.T.R., Mello, C.V., Weir, J.T., Haussler, D., Li, Q., Yang, H., Wang, J., Lei, F., Rahbek, C., Gilbert, M.T.P., Graves, G.R., Jarvis, E.D., Paten, B., Zhang, G., 2020. Dense sampling of bird diversity increases power of comparative genomics. *Nature* 587 (7833), 252–257.
- Field, D.J., Berv, J.S., Hsiang, A.Y., Lanfear, R., Landis, M.J., Dornburg, A., 2020. Timing the extant avian radiation: the rise of modern birds, and the importance of modeling molecular rate variation. In: Pittman, M., Xu, X. (Eds.), *Pennaraptoran Theropod Dinosaurs: Past Progress and New Frontiers*, pages 159–182. Bull. Am. Mus. Nat. Hist. 440.
- Freyman, W.A., 2015. SUMAC: constructing phylogenetic supermatrices and assessing partially decisive taxon coverage. *Evol. Bioinform.* 11, 263–266.
- Friedman, M., Keck, B.P., Dornburg, A., Eytan, R.I., Martin, C.H., Hulsey, C.D., Wainwright, P.C., Near, T.J., 2013. Molecular and fossil evidence place the origin of cichlid fishes long after Gondwanan rifting. *Proc. R. Soc. Lond. B* 280 (1770), 20131733.
- Friesen, V.L., Baker, A.J., Piatt, J.F., 1996. Phylogenetic relationships within the Alcidae (Charadriiformes: Aves) inferred from total molecular evidence. *Mol. Biol. Evol.* 13 (2), 359–367.
- Galla, S.J., Forsück, N.J., Brown, L., Hoeppner, M.P., Knapp, M., Maloney, R.F., Moraga, R., Santure, A.W., Steeves, T.E., 2019. Reference genomes from distantly related species can be used for discovery of single nucleotide polymorphisms to inform conservation management. *Genes* 10 (1), 9.
- García-R, J.C., Gibb, G.C., Trewick, S.A., 2014. Deep global evolutionary radiation in birds: Diversification and trait evolution in the cosmopolitan bird family Rallidae. *Mol. Phylogenet. Evol.* 81, 96–108.
- Gatesy, J., Springer, M.S., 2004. A critique of matrix representation with parsimony supertrees. In: Bininda-Emonds, O.R.P. (Ed.), *Phylogenetic Supertrees: Combining Information to Reveal the Tree of Life*. Kluwer Academic Publishers, Dordrecht, NL, pp. 369–388.
- Gibson, R., Baker, A.J., 2012. Multiple gene sequences resolve phylogenetic relationships in the shorebird suborder Scopocapi (Aves: Charadriiformes). *Mol. Phylogenet. Evol.* 64 (1), 66–72.
- Gray, G.R., 1840. A list of the genera of birds with an indication of the typical species of each genus. R. & J.E. Taylor, London, UK.
- Gysels, H., Rabaeij, M., 1964. Taxonomic relationships of *Alca torda*, *Fratercula arctica* and *Uria aalge* as revealed by biochemical methods. *Ibis* 106 (4), 536–540.
- Hackett, S.J., Kimball, R.T., Reddy, S., Bowie, R.C.K., Braun, E.L., Braun, M.J., Chojnowski, J.L., Cox, W.A., Han, K.-L., Harshman, J., Huddleston, C.J., Marks, B.D., Miglia, K.J., Moore, W.S., Sheldon, F.H., Steadman, D.W., Witt, C.C., Yuri, T., 2008. A phylogenomic study of birds reveals their evolutionary history. *Science* 320 (5884), 1763–1768.
- Hedman, M.M., 2010. Constraints on clade ages from fossil outgroups. *Paleobiol.* 36 (1), 16–31.
- Heingård, M., Musser, G., Hall, S.A., Clarke, J.A., 2021. New remains of *Scandavis mikkelsenii* inform avian phylogenetic relationships and brain evolution. *Diversity* 13 (12), 651.
- Heled, J., Bouckaert, R.R., 2013. Looking for trees in the forest: summary tree from posterior samples. *BMC Evol. Biol.* 13 (1), 221.
- Hood, S.C., Torres, C.R., Norell, M.A., Clarke, J.A., 2019. New fossil birds from the earliest Eocene of Mongolia. *Am. Mus. Nov.* 2019 (3934), 1–24.
- Hope, S., 2002. The Mesozoic radiation of Neornithes. In: Chiappe, L.M., Witmer, L.M. (Eds.), *Mesozoic Birds: Above the Heads of Dinosaurs*. University of California Press, Berkeley, CA, pp. 339–388.
- Houde, P., Braun, E.L., Narula, N., Minjares, U., Mirarab, S., 2019. Phylogenetic signal of indels and the neoavian radiation. *Diversity* 11 (7), 108.
- Hu, C., Zhang, C., Sun, L., Zhang, Y., Xie, W., Zhang, B., Chang, Q., 2017. The mitochondrial genome of pin-tailed snipe *Gallinago stenura*, and its implications for the phylogeny of Charadriiformes. *PLoS ONE* 12 (4), e0175244.
- Jansen, J.J.F.J., Kamminga, P., Arguello, M., 2021. Taxonomic implications of the original illustrations of *Prosobonia* from Tahiti and Moorea made during the second and third Cook expeditions. *Bull. Br. Orn. Club* 141 (2), 133–141.
- Jarvis, E.D., Mirarab, S., Aberer, A.J., Li, B., Houde, P., Li, C., Ho, S.Y.W., Faircloth, B.C., Nabholz, B., Howard, J.T., Suh, A., Weber, C.C., da Fonseca, R.R., Li, J., Zhang, F., Li, H., Zhou, L., Narula, N., Liu, L., Ganapathy, G., Boussau, B., Bayzid, M.S., Zavidovych, V., Subramanian, S., Gabaldón, T., Capella-Gutiérrez, S., Huerta-Cepas, J., Rekpelchi, B., Munch, K., Schierup, M., Lindow, B., Warren, W.C., Ray, D., Green, R.E., Bruford, M.W., Zhan, X., Dixon, A., Li, S., Li, N., Huang, Y., Berryberry, E.P., Bertelsen, M.F., Sheldon, F.H., Brumfield, R.T., Mello, C.V., Lovell, P.V., Wirthlin, M., Schneider, M.P.C., Prosdocimi, F., Samaniego, J.A., Velazquez, A.M.V., Alfaro-Núñez, A., Campos, P.F., Petersen, B., Sicheritz-Ponten, T., Pas, A., Bailey, T., Scofield, P., Bunce, M., Lambert, D.M., Zhou, Q., Perelman, P., Driskell, A.C., Shapiro, B., Xiong, Z., Zeng, Y., Liu, S., Li, Z., Liu, B., Wu, K., Xiao, J., Yinqi, X., Zheng, Q., Zhang, Y., Yang, H., Wang, J., Smeds, L., Rheindt, F.E., Braun, M., Fjeldså, J., Orlando, L., Barker, F.K., Jonsson, K.A., Johnson, W., Koepfl, K.-P., O'Brien, S., Haussler, D., Ryder, O.A., Rahbek, C., Willerslev, E., Graves, G.R., Glenn, T.C., McCormack, J., Burt, D., Ellegren, H., Alström, P., Edwards, S.V., Stamatakis, A., Mindell, D.P., Cracraft, J., Braun, E.L., Warnow, T., Jun, W., Gilbert, M.T.P., Zhang, G., 2014. Whole-genome analyses resolve early branches in the tree of life of modern birds. *Science*, 346(6215):1320–1331.
- Jehl, J.R., 1968. The systematic position of the Surfbird, *Aphriza virgata*. *Condor* 70 (3), 206–210.
- Jetz, W., Thomas, G.H., Joy, J.B., Hartmann, K., Mooers, A.O., 2012. The global diversity of birds in space and time. *Nature* 491 (7424), 444–448.
- Joseph, L., Lessa, E.P., Christidis, L., 1999. Phylogeny and biogeography in the evolution of migration: shorebirds of the *Charadrius* complex. *J. Biogeogr.* 26 (2), 329–342.
- Kass, R.E., Raftery, A.E., 1995. Bayes factors. *J. Am. Stat. Assoc.* 90 (430), 773–795.
- Kearse, M., Moir, R., Wilson, A., Stones-Havas, S., Cheung, M., Sturrock, S., Buxton, S., Cooper, A., Markowitz, S., Duran, C., Thaler, T., Ashton, B., Meintjes, P., Drummond, A., 2012. Geneious Basic: An integrated and extendable desktop software platform for the organization and analysis of sequence data. *Bioinform.* 28 (12), 1647–1649.
- Kimball, R.T., Oliveros, C.H., Wang, N., White, N.D., Barker, F.K., Field, D.J., Ksepka, D.T., Chesser, R.T., Moyle, R.G., Braun, M.J., Brumfield, R.T., Faircloth, B.C., Smith, B.T., Braun, E.L., 2019. A phylogenomic supertree of birds. *Diversity* 11 (7), 109.
- Kimball, R.T., Wang, N., Heimer-McGinn, V., Ferguson, C., Braun, E.L., 2013. Identifying localized biases in large datasets: A case study using the avian tree of life. *Mol. Phylogenet. Evol.* 69 (3), 1021–1032.
- Kishino, H., Hasegawa, M., 1989. Evaluation of the maximum likelihood estimate of the evolutionary tree topologies from DNA sequence data, and the branching order in Hominoidea. *J. Mol. Evol.* 29 (2), 170–179.
- Kobert, K., Salichos, L., Rokas, A., Stamatakis, A., 2016. Computing the internode certainty and related measures from partial gene trees. *Mol. Biol. Evol.* 33 (6), 1606–1617.
- Kozlov, A.M., Darriba, D., Flouri, T., Morel, B., Stamatakis, A., 2019. RAxML-NG: a fast, scalable and user-friendly tool for maximum likelihood phylogenetic inference. *Bioinform.* 35 (21), 4453–4455.
- Kozlova, E.V., 1961. Fauna of USSR: Birds. Volume II No. 3. Charadriiformes, Suborder Alcae [Translation by R. Ettinger]. Israel Program for Scientific Translations, Jerusalem.
- Krajewski, C., Sipiorski, J.T., Anderson, F.E., 2010. Complete mitochondrial genome sequences and the phylogeny of cranes (Gruiformes: Gruidae). *Auk* 127 (2), 440–452.
- Ksepka, D.T., Phillips, M.J., 2015. Avian diversification patterns across the K-Pg boundary: influence of calibrations, datasets, and model misspecification. *Ann. Missouri Bot. Gard.* 100 (4), 300–328.
- Ksepka, D.T., Stidham, T.A., Williamson, T.E., 2017. Early Paleocene landbird supports rapid phylogenetic and morphological diversification of crown birds after the K-Pg mass extinction. *Proc. Natl. Acad. Sci. USA* 114 (30), 8047–8052.
- Kuhl, H., Frankl-Vilches, C., Bakker, A., Mayr, G., Nikolaus, G., Boerner, S.T., Klages, S., Timmermann, B., Gahr, M., 2020. An unbiased molecular approach using 3'-UTRs resolves the avian family-level tree of life. *Mol. Biol. Evol.* 38 (1), 108–127.
- Lanfear, R., Frandsen, P.B., Wright, A.M., Senfeld, T., Calcott, B., 2016. PartitionFinder 2: new methods for selecting partitioned models of evolution for molecular and morphological phylogenetic analyses. *Mol. Biol. Evol.* 34 (3), 772–773.
- Lanyon, S.M., 1988. The stochastic mode of molecular evolution: What consequences for systematic investigations? *Auk* 105 (3), 565–573.
- Larsson, A., 2014. AliView: a fast and lightweight alignment viewer and editor for large datasets. *Bioinform.* 30 (22), 3276–3278.
- Lewis, P.O., 2001. A likelihood approach to estimating phylogeny from discrete morphological character data. *Syst. Biol.* 50 (6), 913–925.
- Li, H.-T., Yi, T.-S., Gao, L.-M., Ma, P.-F., Zhang, T., Yang, J.-B., Gitzendanner, M.A., Fritsch, P.W., Cai, J., Luo, Y., Wang, H., van der Bank, M., Zhang, S.-D., Wang, Q.-F., Wang, J., Zhang, Z.-R., Fu, C.-N., Yang, J., Hollingsworth, P.M., Chase, M.W., Soltis, D.E., Soltis, P.S., Li, D.-Z., 2019. Origin of angiosperms and the puzzle of the Jurassic gap. *Nature Plants* 5 (5), 461–470.
- Livezey, B.C., 2010. Phylogenetics of modern shorebirds (Charadriiformes) based on phenotypic evidence: analysis and discussion. *Zool. J. Linn. Soc.* 160 (3), 567–618.
- Livezey, B.C., Zusi, R.L., 2007. Higher-order phylogeny of modern birds (Theropoda, Aves: Neornithes) based on comparative anatomy. II. Analysis and discussion. *Zool. J. Linn. Soc.* 149 (1), 1–95.

- Makowski, D., Ben-Shachar, M.S., Lüdecke, D., 2019. bayestestR: Describing effects and their uncertainty, existence and significance within the Bayesian framework. *J. Open Source Softw.* 4 (40), 1541.
- Marki, P.Z., Jonsson, K.A., Irestedt, M., Nguyen, J.M.T., Rahbek, C., Fjeldså, J., 2017. Supermatrix phylogeny and biogeography of the Australasian Meliphagidae radiation (Aves: Passeriformes). *Mol. Phylogenet. Evol.* 107, 516–529.
- Maurin, K.J.L., 2020. An empirical guide for producing a dated phylogeny with treePL in a maximum likelihood framework. *arXiv* 2008.07054v2.
- Mayr, G., 2000. Charadriiform birds from the early Oligocene of Céreste (France) and the Middle Eocene of Messel (Hessen, Germany). *Geobios* 33 (5), 625–636.
- Mayr, G., 2009. Paleogene Fossil Birds. Springer-Verlag, Berlin, Germany.
- Mayr, G., 2011. The phylogeny of charadriiform birds (shorebirds and allies) – reassessing the conflict between morphology and molecules. *Zool. J. Linn. Soc.* 161 (4), 916–934.
- Mayr, G., 2014. The origins of crown group birds: molecules and fossils. *Palaeontol.* 57 (2), 231–242.
- Mayr, G., 2016. The world's smallest owl, the earliest unambiguous charadriiform bird, and other avian remains from the early Eocene Nanjemoy Formation of Virginia (USA). *PalZ* 90 (4), 747–763.
- McCormack, J.E., Harvey, M.G., Faircloth, B.C., Crawford, N.G., Glenn, T.C., Brumfield, R.T., 2013. A phylogeny of birds based on over 1,500 loci collected by target enrichment and high-throughput sequencing. *PLoS ONE* 8 (1), 1–11.
- McCraney, W.T., Thacker, C.E.T., Alfaro, M.E., 2020. Supermatrix phylogeny resolves goby lineages and reveals unstable root of Gobiaria. *Mol. Phylogenet. Evol.* 151, 106862.
- McKittrick, M.C., 1991. Phylogenetic analysis of avian hindlimb musculature. *Misc. Pub. Mus. Zool. U. Michigan* 179, 1–87.
- Miller, E.H., Areta, J.I., Jaramillo, A., Imberti, S., Matus, R., 2020. Snipe taxonomy based on vocal and non-vocal sound displays: the South American Snipe is two species. *Ibis* 162 (3), 968–990.
- Miller, M.A., Pfeiffer, W., Schwartz, T., 2010. Creating the CIPRES Science Gateway for inference of large phylogenetic trees. In: Proceedings of the Gateway Computing Environments Workshop (GCE). IEEE Press, New Orleans, LA, pp. 1–8.
- Minh, B.Q., Schmidt, H.A., Chernomor, O., Schrempf, D., Woodhams, M.D., von Haeseler, A., Lanfear, R., 2020. IQ-TREE 2: new models and efficient methods for phylogenetic inference in the genomic era. *Mol. Biol. Evol.* 37 (5), 1530–1534.
- Mirarab, S., Bayzid, M.S., Warnow, T., 2016. Evaluating summary methods for multilocus species tree estimation in the presence of incomplete lineage sorting. *Syst. Biol.* 65 (3), 366–380.
- Mirarab, S., Reaz, R., Bayzid, M.S., Zimmermann, T., Swenson, M.S., Warnow, T., 2014. ASTRAL: genome-scale coalescent-based species tree estimation. *Bioinform.* 30 (17), i541–i548.
- Mitchell, J.S., Etienne, R.S., Rabosky, D.L., 2018. Inferring diversification rate variation from phylogenies with fossils. *Syst. Biol.* 68 (1), 1–18.
- Moum, T., Johansen, S., Erikstad, K.E., Piatt, J.F., 1994. Phylogeny and evolution of the auks (subfamily Alcinae) based on mitochondrial DNA sequences. *Proc. Natl. Acad. Sci. USA* 91 (17), 7912–7916.
- Moynihan, M., 1959. A revision of the family Laridae (Aves). *Am. Mus. Nov.* 1928, 1–42.
- Musser, G., Clarke, J.A., 2020. An exceptionally preserved specimen from the Green River Formation elucidates complex phenotypic evolution in Gruiformes and Charadriiformes. *Front. Ecol. Evol.* 8, 559929.
- Musser, G., Ksepka, D.T., Field, D.J., 2019. New material of Paleocene-Eocene *Pellornis* (Aves: Gruiformes) clarifies the pattern and timing of the extant gruiform radiation. *Diversity* 11 (7), 102.
- Nielsen, B.P., 1975. Affinities of *Eudromias morinellus* (L.) to the genus *Charadrius* L. *Ornis Scand.* 6 (1), 65–82.
- Olson, S.L., Steadman, D.W., 1981. The relationships of the Pedionomidae (Aves, Charadriiformes). *Smithson. Contrib. Zool.* 337, 1–25.
- Olsson, U., Alström, P., 2020. A comprehensive phylogeny and taxonomic evaluation of the waxbills (Aves: Estrildidae). *Mol. Phylogenet. Evol.* 146, 106757.
- Päckert, M., 2022. Free access of published DNA sequences facilitates regular control of (meta-) data quality – an example from shorebird mitogenomes (Aves, Charadriiformes: *Charadrius*). *Ibis* 164 (1), 336–342.
- Parham, J.F., Donoghue, P.C.J., Bell, C.J., Calway, T.D., Head, J.J., Holroyd, P.A., Inoue, J.G., Irmis, R.B., Joyce, W.G., Ksepka, D.T., Patané, J.S.L., Smith, N.D., Tarver, J.E., van Tuinen, M., Yang, Z., Angielczyk, K.D., Greenwood, J.M., Hipsley, C.A., Jacobs, L., Makovicky, P.J., Müller, J., Smith, K.T., Theodor, J.M., Warnock, R.C.M., Benton, M.J., 2011. Best practices for justifying fossil calibrations. *Syst. Biol.* 61 (2), 346–359.
- Paton, T., Haddrath, O., Baker, A.J., 2002. Complete mitochondrial DNA genome sequences show that modern birds are not descended from transitional shorebirds. *Proc. R. Soc. Lond. B* 269 (1493), 839–846.
- Paton, T.A., Baker, A.J., 2006. Sequences from 14 mitochondrial genes provide a well-supported phylogeny of the Charadriiform birds congruent with the nuclear RAG-1 tree. *Mol. Phylogenet. Evol.* 39 (3), 657–667.
- Paton, T.A., Baker, A.J., Groth, J.G., Barrowclough, G.F., 2003. RAG-1 sequences resolve phylogenetic relationships within Charadriiform birds. *Mol. Phylogenet. Evol.* 29 (2), 268–278.
- Pattengale, N.D., Alipour, M., Bininda-Emonds, O.R.P., Moret, B.M.E., Stamatakis, A., 2010. How many bootstrap replicates are necessary? *J. Comp. Biol.* 17 (3), 337–354.
- Pereira, S.L., Baker, A.J., 2006. A mitogenomic timescale for birds detects variable phylogenetic rates of molecular evolution and refutes the standard molecular clock. *Mol. Biol. Evol.* 23 (9), 1731–1740.
- Pereira, S.L., Baker, A.J., 2008. DNA evidence for a Paleocene origin of the Alcidae (Aves: Charadriiformes) in the Pacific and multiple dispersals across northern oceans. *Mol. Phylogenet. Evol.* 46 (2), 430–445.
- Pereira, S.L., Baker, A.J., 2010. The enigmatic monotypic crab plover *Dromas ardeola* is closely related to pratincoles and coursers (Aves, Charadriiformes, Glareolidae). *Genet. Mol. Biol.* 33 (3), 583–586.
- Plummer, M., Best, N., Cowles, K., Vines, K., 2006. CODA: Convergence Diagnosis and Output Analysis for MCMC. *R News* 6, 7–11.
- Pons, J.-M., Hassanin, A., Crochet, P.-A., 2005. Phylogenetic relationships within the Laridae (Charadriiformes: Aves) inferred from mitochondrial markers. *Mol. Phylogenet. Evol.* 37 (3), 686–699.
- Prum, R.O., Berv, J.S., Dornburg, A., Field, D.J., Townsend, J.P., Lemmon, E.M., Lemmon, A.R., 2015. A comprehensive phylogeny of birds (Aves) using targeted next-generation DNA sequencing. *Nature* 526 (7574), 569–573.
- Quoy, J.R.C., Gaimard, J.P., 1832. Voyage de découvertes de l'Astrolabe: exécuté par ordre du Roi, pendant les années 1826–1827–1828–1829, sous le commandement de M. J. Dumont d'Urville. Troisième Divison: Zoologie. Tome Premier. J. Tastu, Paris, France.
- R Core Team, 2019. R: A Language and Environment for Statistical Computing. R Foundation for Statistical Computing, Vienna, Austria.
- Rabosky, D.L., 2014. Automatic detection of key innovations, rate shifts, and diversity-dependence on phylogenetic trees. *PLOS ONE* 9 (2), e89543.
- Rabosky, D.L., 2015. No substitute for real data: A cautionary note on the use of phylogenies from birth–death polytomous resolvers for downstream comparative analyses. *Evolution* 69 (12), 3207–3216.
- Rabosky, D.L., Grindler, M., Anderson, C., Title, P., Shi, J.J., Brown, J.W., Huang, H., Larson, J.G., 2014. BAMMtools: an R package for the analysis of evolutionary dynamics on phylogenetic trees. *Methods Ecol. Evol.* 5 (7), 701–707.
- Rambaut, A., Drummond, A.J., Xie, D., Baele, G., Suchard, M.A., 2018. Posterior summarization in Bayesian phylogenetics using Tracer 1.7. *Syst. Biol.* 67 (5), 901–904.
- Ratnasingham, S., Hebert, P.D.N., 2007. BOLD: The Barcode of Life Data System (<http://www.barcodinglife.org>). *Mol. Ecol. Notes* 7 (3), 355–364.
- Reddy, S., Kimball, R.T., Pandey, A., Hosner, P.A., Braun, M.J., Hackett, S.J., Han, K.-L., Harshman, J., Huddleston, C.J., Kingston, S., Marks, B.D., Miglia, K.J., Moore, W.S., Sheldon, F.H., Witt, C.C., Yuri, T., Braun, E.L., 2017. Why do phylogenomic data sets yield conflicting trees? Data type influences the avian tree of life more than taxon sampling. *Syst. Biol.* 66 (5), 857–879.
- Reyes, A., Gissi, C., Catzeffis, F., Nevo, E., Pesole, G., Saccone, C., 2004. Congruent mammalian trees from mitochondrial and nuclear genes using Bayesian methods. *Mol. Biol. Evol.* 21 (2), 397–403.
- Robinson, D.F., Foulds, L.R., 1981. Comparison of phylogenetic trees. *Math. Biosci.* 53 (1–2), 131–147.
- Ronquist, F., Teslenko, M., van der Mark, P., Ayres, D.L., Darling, A., Höhna, S., Larget, B., Liu, L., Suchard, M.A., Huelsenbeck, J.P., 2012. MrBayes 3.2: Efficient Bayesian phylogenetic inference and model choice across a large model space. *Syst. Biol.* 61 (3), 539–542.
- Roquet, C., Smyčka, J., Alberti, A., Boleda, M., Coissac, E., Denoeud, F., Komac, B., Lavergne, S., Pladevall, C., Sáez, L., 2022. Evolutionary origins and species delineation of the two pyrenean endemics *Campanula jaubertiana* and *C. andorrana* (Campanulaceae): evidence for transverse alpine speciation. *Alp. Bot.* 132 (1), 51–64.
- Rotthowe, K., Starck, J.M., 1998. Evidence for a phylogenetic position of button quails (Turnicidae: Aves) among the Gruiformes. *J. Zool. Syst. Evol. Res.* 36 (1–2), 39–51.
- Sadanandan, K.R., Küpper, C., Low, G.W., Yao, C.-T., Li, Y., Xu, T., Rheindt, F.E., Wu, S., 2019. Population divergence and gene flow in two East Asian shorebirds on the verge of speciation. *Sci. Reports* 9 (1), 8546.
- Salichos, L., Rokas, A., 2013. Inferring ancient divergences requires genes with strong phylogenetic signals. *Nature* 497 (7449), 327–331.
- Salichos, L., Stamatakis, A., Rokas, A., 2014. Novel information theory-based measures for quantifying incongruence among phylogenetic trees. *Mol. Biol. Evol.* 31 (5), 1261–1271.
- Sanderson, M.J., 2002. Estimating absolute rates of molecular evolution and divergence times: a penalized likelihood approach. *Mol. Biol. Evol.* 19 (1), 101–109.
- Sanderson, M.J., McMahon, M.M., Steel, M., 2010. Phylogenomics with incomplete taxon coverage: the limits to inference. *BMC Evol. Biol.* 10 (1), 155.
- Sangster, G., Luksenburg, J.A., 2021. Sharp increase of problematic mitogenomes of birds: Causes, consequences, and remedies. *Genome Biol. Evol.* 13 (9), evab210.
- Sayyari, E., Mirarab, S., 2016. Fast coalescent-based computation of local branch support from quartet frequencies. *Mol. Biol. Evol.* 33 (7), 1654–1668.
- Sayyari, E., Mirarab, S., 2018. Testing for polytomies in phylogenetic species trees using quartet frequencies. *Genes* 9 (3), 132.
- Sayyari, E., Whitfield, J.B., Mirarab, S., 2018. DiscoVista: Interpretable visualizations of gene discordance. *Mol. Phylogenet. Evol.* 122, 110–115.
- Senfeld, T., Shannon, T.J., van Grouw, H., Pajjmans, D.M., Tavares, E.S., Baker, A.J., Lees, A.C., Collinson, J.M., 2020. Taxonomic status of the extinct Canary Islands Oystercatcher *Haematopus meadewaldoi*. *Ibis* 162 (3), 1068–1074.
- Shimodaira, H., 2002. An approximately unbiased test of phylogenetic tree selection. *Syst. Biol.* 51 (3), 492–508.
- Shimodaira, H., Hasegawa, M., 1999. Multiple comparisons of log-likelihoods with applications to phylogenetic inference. *Mol. Biol. Evol.* 16 (8), 1114–1114.
- Sibley, C.G., Ahlquist, J.E., 1990. Phylogeny and Classification of Birds: A Study in Molecular Evolution. Yale University Press, New Haven, CT.
- Simmons, M.P., Springer, M.S., Gatesy, J., 2022. Gene-tree misrooting drives conflicts in phylogenomic coalescent analyses of palaeognath birds. *Mol. Phylogenet. Evol.* 167, 107344.
- Smith, B.T., Klicka, J., 2013. Examining the role of effective population size on mitochondrial and multilocus divergence time discordance in a songbird. *PLOS ONE* 8 (2), e55161.

- Smith, N.A., 2011. Systematics and evolution of extinct and extant Pan-Alcidae (Aves, Charadriiformes): combined phylogenetic analyses, divergence estimation, and paleoclimatic interactions.. PhD thesis. University of Texas at Austin.
- Smith, N.A., 2015. Sixteen vetted fossil calibrations for divergence dating of Charadriiformes (Aves, Neognathae). *Palaeont. Elec.*, 18(1.4FC).
- Smith, N.A., Clarke, J.A., 2012. Endocranial anatomy of the Charadriiformes: sensory system variation and the evolution of wing-propelled diving. *PLoS ONE* 7 (11), e49584.
- Smith, N.A., Clarke, J.A., 2015. Systematics and evolution of the Pan-Alcidae (Aves, Charadriiformes). *J. Avian Biol.* 46 (2), 125–140.
- Smith, S.A., O'Meara, B.C., 2012. treePL: divergence time estimation using penalized likelihood for large phylogenies. *Bioinform.* 28 (20), 2689–2690.
- Springer, M.S., Emerling, C.A., Meredith, R.W., Janecka, J.E., Eizirik, E., Murphy, W.J., 2017. Waking the undead: Implications of a soft explosive model for the timing of placental mammal diversification. *Mol. Phylogenet. Evol.* 106, 86–102.
- Springer, M.S., Gatesy, J., 2018. Delimiting coalescence genes (c-genes) in phylogenomic data sets. *Genes* 9 (3), 123.
- Stamatakis, A., 2014. RAxML version 8: a tool for phylogenetic analysis and post-analysis of large phylogenies. *Bioinform.* 30 (9), 1312–1313.
- Stein, R.W., Mull, C.G., Kuhn, T.S., Aschliman, N.C., Davidson, L.N.K., Joy, J.B., Smith, G.J., Dulvy, N.K., Mooers, A.Ø., 2018. Global priorities for conserving the evolutionary history of sharks, rays and chimaeras. *Nature Ecol. Evol.* 2 (2), 288–298.
- Storer, R.W., 1960. Evolution in the diving birds. In: Bergman, G., Donner, K.O., von Haartman, L. (Eds.), *Proceedings of the XII International Ornithological Congress*, pages 694–707. Tilgmannin Kirjapaino, Helsinki.
- Strauch Jr., J.G., 1978. The phylogeny of the Charadriiformes (Aves): a new estimate using the method of character compatibility analysis. *Trans. Zool. Soc. Lond.* 34 (3), 263–345.
- Strauch Jr., J.G., 1985. The phylogeny of the Alcidae. *Auk* 102 (3), 520–539.
- Strimmer, K., Rambaut, A., 2002. Inferring confidence sets of possibly misspecified gene trees. *Proc. R. Soc. Lond. B* 269 (1487), 137–142.
- Suh, A., 2016. The phylogenomic forest of bird trees contains a hard polytomy at the root of Neoaves. *Zool. Scr.* 45 (S1), 50–62.
- Suh, A., Smeds, L., Ellegren, H., 2015. The dynamics of incomplete lineage sorting across the ancient adaptive radiation of neoavian birds. *PLOS Biol.* 13 (8), e1002224.
- Thomas, G.H., Wills, M.A., Székely, T., 2004. A supertree approach to shorebird phylogeny. *BMC Evol. Biol.* 4 (1), 28.
- Upham, N.S., Esselstyn, J.A., Jetz, W., 2021. Molecules and fossils tell distinct yet complementary stories of mammal diversification. *Curr. Biol.* 31 (19), 4195–4206.e3.
- Verheyen, R., 1958. Analyse du potentiel morphologique et projet d'une nouvelle classification des charadriiformes. *Bull. Inst. roy. Sci. nat. Belg.* 34 (18), 1–35.
- Wahlsteen, E., Zhou, W., Xiang, Q., Rushforth, K., 2021. Rediscovery of the lost little dogwood *Cornus wardiana* (Cornaceae)—Its phylogenetic and morphological distinction and implication in the origin of the Arctic-Sino-Himalayan disjunction. *J. Syst. Evol.* 59 (2), 405–416.
- Wang, X., Maher, K.H., Zhang, N., Que, P., Zheng, C., Liu, S., Wang, B., Huang, Q., Chen, D., Yang, X., Zhang, Z., Székely, T., Urrutia, A.O., Liu, Y., 2019a. Demographic histories and genome-wide patterns of divergence in incipient species of shorebirds. *Front. Genet.* 10, 919.
- Wang, X., Que, P., Heckel, G., Hu, J., Zhang, X., Chiang, C.-Y., Zhang, N., Huang, Q., Liu, S., Martinez, J., Pagani-Núnez, E., Dingle, C., Leung, Y.Y., Székely, T., Zhang, Z., Liu, Y., 2019b. Genetic, phenotypic and ecological differentiation suggests incipient speciation in two *Charadrius* plovers along the Chinese coast. *BMC Evol. Biol.* 19 (1), 135.
- Weedop, K.B., Mooers, A.Ø., Tucker, C.M., Pearse, W.D., 2019. The effect of phylogenetic uncertainty and imputation on EDGE Scores. *Anim. Conserv.* 22 (6), 527–536.
- Wetmore, A., 1960. A classification for the birds of the world. *Smithson. Misc. Coll.* 139 (11), 1–37.
- Whitfield, J.B., Lockhart, P.J., 2007. Deciphering ancient rapid radiations. *Trends Ecol. Evol.* 22 (5), 258–265.
- Whittingham, L.A., Sheldon, F.H., Emlen, S.T., 2000. Molecular phylogeny of jacanas and its implications for morphologic and biogeographic evolution. *Auk* 117 (1), 22–32.
- Wilkinson, R.D., Steiper, M.E., Soligo, C., Martin, R.D., Yang, Z., Tavaré, S., 2010. Dating primate divergences through an integrated analysis of palaeontological and molecular data. *Syst. Biol.* 60 (1), 16–31.
- Yang, Z., 2007. PAML 4: Phylogenetic Analysis by Maximum Likelihood. *Mol. Biol. Evol.* 24 (8), 1586–1591.
- Yang, Z., 2014. *Molecular Evolution: A Statistical Approach*. Oxford University Press, Oxford, UK.
- Yang, Z., Rannala, B., 2005. Bayesian estimation of species divergence times under a molecular clock using multiple fossil calibrations with soft bounds. *Mol. Biol. Evol.* 23 (1), 212–226.
- Yuri, T., Kimball, R.T., Harshman, J., Bowie, R.C.K., Braun, M.J., Chojnowski, J.L., Han, K.-L., Hackett, S.J., Huddleston, C.J., Moore, W.S., Reddy, S., Sheldon, F.H., Steadman, D.W., Witt, C.C., Braun, E.L., 2013. Parsimony and model-based analyses of indels in avian nuclear genes reveal congruent and incongruent phylogenetic signals. *Biology* 2 (1), 419–444.
- Zaher, H., Murphy, R.W., Arredondo, J.C., Graboski, R., Machado-Filho, P.R., Mahlow, K., Montingelli, G.G., Quadros, A.B., Orlov, N.L., Wilkinson, M., Zhang, Y.-P., Grazziotin, F.G., 2019. Large-scale molecular phylogeny, morphology, divergence-time estimation, and the fossil record of advanced caenophidian snakes (Squamata: Serpentes). *PLOS ONE* 14 (5), e0216148.
- Zhang, C., Rabiee, M., Sayyari, E., Mirarab, S., 2018. ASTRAL-III: polynomial time species tree reconstruction from partially resolved gene trees. *BMC Bioinform.* 19, 153.
- Zhang, G., Li, B., Li, C., Gilbert, M.T.P., Jarvis, E.D., Wang, J., Consortium, T.A.G., 2014. Comparative genomic data of the Avian Phylogenomics Project. *GigaScience* 3 (1), 2047-217X-3-26.
- Zheng, Y., Peng, R., Kuro-o, M., Zeng, X., 2011. Exploring patterns and extent of bias in estimating divergence time from mitochondrial DNA sequence data in a particular lineage: a case study of salamanders (order Caudata). *Mol. Biol. Evol.* 28 (9), 2521–2535.